

Diffusion and Lyapunov timescales in the Arnold model

Pablo M. Cincotta ^{*}

*Grupo de Caos en Sistemas Hamiltonianos, Facultad de Ciencias Astronómicas y Geofísicas,
Universidad Nacional de La Plata and Instituto de Astrofísica de La Plata (CONICET), B1900FWA La Plata, Argentina*

Claudia M. Giordano [†]

*Grupo de Caos en Sistemas Hamiltonianos, Facultad de Ciencias Astronómicas y Geofísicas,
Universidad Nacional de La Plata and Instituto de Astrofísica de La Plata (CONICET), B1900FWA La Plata, Argentina*

Ivan I. Shevchenko [‡]

*Saint Petersburg State University, 7/9 Universitetskaya nab., 199034 Saint Petersburg, Russia
and Institute of Applied Astronomy, RAS, 191187 Saint Petersburg, Russia*



(Received 30 August 2022; accepted 26 September 2022; published 13 October 2022)

In the present work, we focus on two dynamical timescales in the Arnold Hamiltonian model: the Lyapunov time and the diffusion time when the system is confined to the stochastic layer of its dominant resonance (guiding resonance). Following Chirikov's formulation, the model is revisited, and a discussion about the main assumptions behind the analytical estimates for the diffusion rate is given. On the other hand, and in line with Chirikov's ideas, theoretical estimations of the Lyapunov time are derived. Later on, three series of numerical experiments are presented for various sets of values of the model parameters, where both timescales are computed. Comparisons between the analytical estimates and the numerical determinations are provided whenever the parameters are not too large, and those cases are in fact in agreement. In particular, the case in which both parameters are equal is numerically investigated. Relationships between the diffusion time and the Lyapunov time are established, like an exponential law or a power law in the case of large values of the parameters.

DOI: [10.1103/PhysRevE.106.044205](https://doi.org/10.1103/PhysRevE.106.044205)

I. INTRODUCTION

The diffusion time, T_D , usually defined heuristically in chaotic dynamics as the timescale for significant variations of the integrals of motion, plays a crucial role in dynamical systems, in particular in Hamiltonian ones. In a broad sense, it determines how long a system could last in its present configuration. On the other hand, the Lyapunov time, T_L , defined as the inverse of the maximum Lyapunov exponent, determines a timescale for the system's chaotic behavior to manifest.

Consider a near-integrable Hamiltonian, $H = H_0 + \varepsilon V$, where H_0 is the integrable part and εV is the perturbation.

Analytical estimates of $T_D(\varepsilon)$ can be obtained under severe restrictions, in general when $\varepsilon \rightarrow 0$, and thus their applications are rather limited. On the other hand, numerical estimates can be obtained in at least two different ways:

(i) A nearly normal diffusion process can be assumed so that the diffusion coefficient, D , can be derived by a linear fit on the evolution of the variance of the unperturbed actions over large motion times being $T_D \sim D^{-1}$. This procedure to determine D is largely used to investigate the global diffusion

process in many different dynamical systems, as, for instance, in Refs. [1–9].

(ii) Alternatively, T_D can be estimated from direct numerical simulations as the required motion time for a prescribed (not small) variation of the actions, as was done, for instance, in Refs. [10–13].

Theoretical estimates of T_L are possible in relatively simple and low-dimensional systems, where the maximum Lyapunov exponent can be derived under certain plausible assumptions. Therefore, in general T_L should be obtained by numerical means.

A relevant question is whether any relation between the considered timescales can be established. For example, for the standard map, if the stochasticity parameter $K \gg 1$, then the diffusion rate $D \sim K^2$ and the Lyapunov exponent $\sigma \sim \ln(K/2)$ [14], resulting then in the parametric $T_D - T_L$ relation,

$$T_D \sim \exp(-2/T_L).$$

Alternatively, if K is fixed, then in the recurrence statistics the generic quadratic relationship is observed, as is shown in Fig. 4.5 of Ref. [15].

In [16] the parametric relation $T_D - T_L$ is numerically investigated in a biparametric four-dimensional (4D) symplectic map, and the latter depends strongly on the parameters of the model, i.e., if the diffusion is restricted to the stochastic layers

^{*}pmc@fcaglp.unlp.edu.ar

[†]giordano@fcaglp.unlp.edu.ar

[‡]i.shevchenko@spbu.ru

of the resonance web or if it spreads all over the phase space of the system due to a large overlap of resonances.

In this work, we focus on both timescales—the diffusion time and the Lyapunov time—in a relatively simple system of 2.5 degrees of freedom (dof) (or 3 dof in the extended phase space), i.e., the classical Arnold Hamiltonian [17], which is the paradigmatic model to describe the so-called Arnold diffusion. Arnold introduced this Hamiltonian in order to state a mechanism that could drive the diffusion, the so-called Arnold mechanism. The Arnold model was largely investigated, among others, by Chirikov [14] in a more physical than mathematical way, where theoretical estimates of the diffusion rate are given for a very restricted domain of parameter space. As far as we know, numerical studies concerning the diffusion in this model are, at most, scanty. Moreover, estimates of T_L are still lacking.

Therefore, in this effort we investigate numerically both timescales when considering initial conditions such that the system is trapped in a resonance, particularly to the chaotic layer of a main resonance. We will focus on different sets of values of the involved parameters. In one case, the parameters lie in the range where Chirikov's diffusion estimates could apply. Therefore, we discuss the applicability of these estimates and how they should be modified in such a way that, in order of magnitude, they would agree with the numerical results. We also provide, following Chirikov's style, theoretical approximations of T_L and compare them with those obtained numerically. Finally, we investigate whether a parametric $T_D - T_L$ relationship would take place in this specific system considering a wide range of values of the parameters.

In Sec. II the Arnold model is revisited as well as Chirikov's main derivations for the diffusion coefficient [14] and the assumptions behind them. Later on, we discuss the range of applicability of the analytical estimates. In Sec. III the diffusion and Lyapunov timescales are considered, in particular the way in which T_D is numerically computed, and a theoretical estimate of T_L is provided. Comparisons with numerical simulations are included. In Sec. IV numerical experiments are presented for various ranges of the parameter values, in particular when they are comparatively large such that no analytical estimates are available.

II. THE ARNOLD MODEL

Let us consider the Arnold Hamiltonian [14,17], introduced ad hoc to describe the so-called Arnold diffusion. Herein we partially follow the presentation and discussions given in [18].

A. The Hamiltonian and resonance structure

The full Hamiltonian takes the form

$$\begin{aligned} H(I_1, I_2, \vartheta_1, \vartheta_2, t; \varepsilon, \mu) &= \frac{1}{2}(I_1^2 + I_2^2) + \varepsilon(\cos \vartheta_1 - 1)[1 + \mu B(\vartheta_2, t)], \\ B(\vartheta_2, t) &= \sin \vartheta_2 + \cos t, \quad I_1, I_2 \in \mathbb{R}, \\ \vartheta_1, \vartheta_2, t &\in \mathbb{S}^1; \quad \varepsilon \mu \ll \varepsilon \ll 1. \end{aligned} \quad (1)$$

For $\varepsilon \neq 0$, $\mu = 0$, the Hamiltonian (1) becomes

$$\begin{aligned} H_0(I_1, I_2, \vartheta_1; \varepsilon) &= H_1(I_1, \vartheta_1; \varepsilon) + H_2(I_2) \\ &= \frac{1}{2}I_1^2 + \varepsilon(\cos \vartheta_1 - 1) + \frac{1}{2}I_2^2, \end{aligned} \quad (2)$$

so the system has two global integrals,

$$H_1(I_1, \vartheta_1; \varepsilon) = \frac{1}{2}I_1^2 + \varepsilon(\cos \vartheta_1 - 1), \quad H_2(I_2), \quad (3)$$

which determine the invariant tori where the motion proceeds.

Here, H_1 is a pendulum model for the resonance $\omega_1 = 0$ with small oscillation frequency $\omega_0^2 = \varepsilon$. We will refer to this resonance as the guiding resonance.

The minimum and maximum of the pendulum potential are -2ε and 0, respectively. From relation (3) the energy level $H_1 \equiv h_1 = -2\varepsilon$ corresponds to the exact resonance or stable equilibrium point at $(I_1, \vartheta_1) = (0, \pi)$, while $h_1 = 0$ leads to the unstable equilibrium point at $(I_1, \vartheta_1) = (0, 0) \equiv (0, 2\pi)$, and clearly the same energy level corresponds to the separatrix.

The associated frequencies in each degree of freedom are

$$\omega_1 = \omega_p(h_1, \varepsilon), \quad \omega_2 = I_2,$$

where $\omega_p(h_1, \varepsilon)$ is the pendulum frequency,

$$\begin{aligned} \omega_p(h_1, \varepsilon) &= \frac{\pi \omega_0(\varepsilon)}{2K(k_{h_1})}, \quad -2\varepsilon \leq h_1 < 0, \\ \omega_p(h_1, \varepsilon) &= \frac{\pi \omega_r(h_1, \varepsilon)}{2K(k_{h_1}^{-1})}, \quad h_1 > 0; \end{aligned} \quad (4)$$

where $K(\kappa)$ is the complete elliptical integral of the first kind, and

$$k_{h_1}^2 = \frac{h_1 + 2\varepsilon}{2\varepsilon}, \quad \omega_r(h_1, \varepsilon) = \omega_0(\varepsilon)k_{h_1},$$

ω_r being the half-cycle rotation frequency.

In the oscillation regime it is $\omega_p(h_1, \varepsilon) \leq \omega_0(\varepsilon)$. Close to the separatrix for both oscillations and rotations, the frequency $\omega_p(|h_1| \ll 1, \varepsilon) \equiv \omega_{sx}(h_1, \varepsilon)$ takes the asymptotic form

$$\omega_{sx}(h_1, \varepsilon) = \frac{\pi \omega_0(\varepsilon)}{\ln\left(\frac{32\varepsilon}{|h_1|}\right)}, \quad \omega_{sx}(h_1, \varepsilon) \rightarrow 0 \quad \text{as} \quad |h_1| \rightarrow 0. \quad (5)$$

In the rotation regime and for h_1 large enough, it is $2\omega_p(h_1, \varepsilon) \approx \sqrt{2h_1} \approx I_1$.

The guiding resonance $\omega_1 = 0$, whose amplitude is ε , has a half-width $(\Delta I_1)^r = 2\sqrt{\varepsilon}$ in action space, so the variation of I_1 is bounded by $|\Delta I_1| \leq 2\sqrt{\varepsilon}$ while I_2 remains constant. Therefore, in (I_1, I_2) space, $\omega_1 \rightarrow \omega_{sx}(h_1, \varepsilon) \rightarrow 0$ when $I_1 \rightarrow 2\sqrt{\varepsilon}$, i.e., at the separatrix.

For $\varepsilon \neq 0$, $\mu \neq 0$, the original system (1) can be rewritten as

$$\begin{aligned} H(I_1, I_2, \vartheta_1, \vartheta_2, t; \varepsilon, \mu) &= H_0(I_1, I_2, \vartheta_1; \varepsilon) + \mu V(\vartheta_1, \vartheta_2, t; \varepsilon), \\ \mu V &= \varepsilon \mu (\sin \vartheta_2 + \cos t)(\cos \vartheta_1 - 1), \end{aligned} \quad (6)$$

where H_0 is given by (2) and $\vartheta_2(t) = \omega_2 t + \vartheta_2^0$, i.e., the unperturbed solution for ϑ_2 . Therefore, the full Hamiltonian is a pendulum model for the guiding resonance $\omega_1 = 0$ and a free rotator coupled by the perturbation $\mu V(\vartheta_1, \vartheta_2, t; \varepsilon)$ that introduces further resonances.

Since V depends on ϑ_1 , ϑ_2 , and t , it affects the phase oscillations within the guiding resonance, with resonant phase ϑ_1 , and its main effect is to produce the stochastic layer around the separatrix of the resonance of width $w_s \ll 1$.

Moreover, due to the dependence of V on ϑ_2 , the perturbation changes not only I_1 but I_2 as well, and then motion along the stochastic layer would proceed. Due to the chaotic character of the motion inside the layer, the variation of I_2 should also be chaotic, giving rise to a diffusion in I_2 . As a consequence, I_2 might change unboundedly, and a gross instability might result for large enough motion times. This is the way in which Arnold diffusion is described in an heuristic way by Chirikov [14]. However, in this model, since the perturbation V vanishes at $(I_1, \vartheta_1) = (0, 0)$, it is possible to build up a transition chain such that if ω_2 is irrational and μ is exponentially small with respect to ε , then all tori defined by $I_1 = 0$, $I_2 = \omega_2 > 0$ are transition tori (see, for instance, Ref. [19]). Roughly speaking, a transition torus is a whiskered torus such that its arriving whisker M^- (or stable manifold) intersects any manifold that is transverse to its departing whisker M^+ (or unstable manifold). Therefore a transition chain is a set of s transition tori such that M_l^+ of the l -transition torus intersects transversally M_{l+1}^- of the $(l+1)$ -transition torus with $l = 1, \dots, s$. Then for large enough t , a neighborhood Ω of $\zeta = (I_1, I_2, \vartheta_1, \vartheta_2) = (0, \omega_2, 0, \vartheta_2)$ on M_0^+ is mapped by the Hamiltonian flow to a neighborhood $U \subset \Omega$ of $\eta = (0, \omega_2', 0, \vartheta_2')$ on M_s^- .

In other words, a “large variation” of I_2 could take place along the resonance whenever the initial conditions are confined to the chaotic layer. Let us state that by “large variation” we mean that I_2 could vary over a finite domain, which does not imply that it can be analytically proved that I_2 changes without any bound.

In the full Hamiltonian (6), however, $\omega_1 = 0$ is just one of the six first-order resonances. Indeed, using simple trigonometric relations, μV could be written as

$$\begin{aligned} \mu V = & \frac{\varepsilon \mu}{2} [\sin(\vartheta_1 + \vartheta_2) + \sin(\vartheta_1 - \vartheta_2) + \cos(\vartheta_1 - t) \\ & - \cos(\vartheta_1 + t) - \sin \vartheta_2 - \cos t], \end{aligned} \quad (7)$$

and thus, averaging out the term $\cos t$, the set of primary resonances at order ε and $\varepsilon \mu$ are

$$\begin{aligned} O(\varepsilon) : & \{\omega_1 = 0\}, \\ O(\mu\varepsilon) : & \{\omega_2 = 0, \quad \omega_1 \pm \omega_2 = 0 \quad \omega_1 \pm 1 = 0\}. \end{aligned} \quad (8)$$

Note that all the resonances involved in μV have the same half-width, $(\Delta I)^r = \sqrt{2\mu\varepsilon} \ll 2\sqrt{\varepsilon}$, which is much smaller than the half-width of the guiding resonance whenever $\mu \ll \varepsilon$.

In (8) but in action or energy space, we should use the approximation $\omega_1 \approx I_1$ in case $I_1 \gg 2\sqrt{\varepsilon}$, $\omega_1 = 2\omega_p(h_1, \varepsilon)$ in case $I_1 < 2\sqrt{\varepsilon}$ ($h_1 < 0$), as given in (4) or $\omega_1 = 2\omega_p(h_1, \varepsilon)$ in case $I_1 \gtrsim 2\sqrt{\varepsilon}$ ($h_1 > 0$).

The resonance lines in frequency space intersect at seven fixed points, namely $(\omega_1, \omega_2) = (0, 0)$, $(0, \pm 1)$, $(\pm 1, \pm 1)$, and hence the diffusion would spread all over this resonance set.

Note that in action space, for $I_1 \lesssim 2\sqrt{\varepsilon}$, since $\omega_1 = \omega_p(h_1, \varepsilon)$ the resonances should not intersect in the same set of points. For instance, the resonances $\omega_1 = \omega_2$, $\omega_1 = \pm 1$ lead

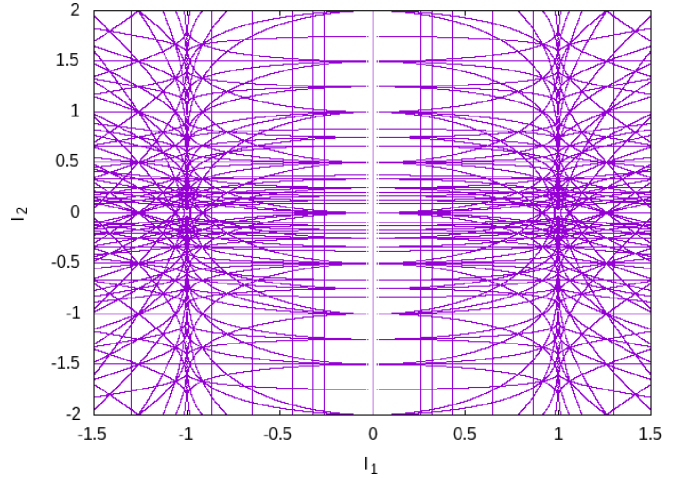


FIG. 1. The Arnold web given by (10) with $\varepsilon = 0.25$ and just for $|m_1| + |m_2| + |m_3| < 6$, where $\omega_1 = \omega_p$ for $|I_1| \leq 2\sqrt{\varepsilon}$ ($h_1 < 0$) while $\omega_1 = 2\omega_p$ for $|I_1| > 2\sqrt{\varepsilon}$ ($h_1 > 0$).

to curves in the (I_1, I_2) plane that change with ε . Indeed, we can take the approximation $\omega_1 \approx \omega_{sx}(h_1, \varepsilon)$ for the half-cycle rotation frequency given by (5) since the system lies outside the pendulum oscillation regime, and the resonance condition $\omega_1(h_1^r, \varepsilon) = 1$ implies $2\omega_{sx}(h_1^r, \varepsilon) \approx 1$, leading to

$$2 \frac{\pi \sqrt{\varepsilon}}{\ln \frac{32\varepsilon}{|h_1^r|}} \approx 1 \rightarrow h_1^r(\varepsilon) \approx 32\varepsilon e^{-2\pi\sqrt{\varepsilon}}.$$

Setting $\vartheta_1 = \pi$ in the expression of H_1 in (3), such that I_1 is taken at the center of the resonance, it follows

$$I_1^r(\varepsilon) \approx \sqrt{2h_1^r(\varepsilon) + 4\varepsilon}. \quad (9)$$

On the other hand, for $I_1 \gg 2\sqrt{\varepsilon}$ both action and frequency spaces are similar.

Considering the perturbed motion, besides the ones given in (8), at first order in ε , the full set of resonances is a linear combination of the form

$$m_1\omega_1 + m_2\omega_2 + m_3 = 0, \quad \forall m_1, m_2, m_3 \in \mathbb{Z} \setminus \{0\}, \quad (10)$$

where again, $\omega_1 \approx I_1$ or $\omega_p(h_1, \varepsilon)$ for oscillations and $2\omega_p(h_1, \varepsilon)$ for rotations, depending on whether $I_1/(2\sqrt{\varepsilon})$ is large or not, respectively.

Figure 1 displays the resonances (10) in action space for $\varepsilon = 0.25$ and $|m_1| + |m_2| + |m_3| < 6$ after setting $\vartheta_1 = \pi$ so that (9) holds. In the figure, the curves represent the relation

$$I_2 = -\frac{m_1}{m_2}\omega_1(I_1) - \frac{m_3}{m_2}, \quad m_2 \neq 0,$$

where $I_2 = \omega_2$, while the vertical lines are given by the approximation $\omega_1 = 2\omega_{sx}$ for $h_1 > 0$. Therefore, all vertical lines correspond to resonances with $m_2 = 0$, the horizontal lines correspond to $m_1 = 0$, and an infinite but countable set of curves for $m_1, m_2 \neq 0$ accumulate toward the separatrix at $I_1^s = 2\sqrt{\varepsilon}$, which for the considered value of ε is $I_1^s = 1$.

B. Diffusion estimates

Chirikov [14] provides estimates of the diffusion rate, $D(I_2, \varepsilon, \mu)$, for the variation of I_2 along the guiding reso-

nance that are only valid whenever both parameters are quite small, i.e., as is customary to say, when the system is in the Nekhoroshev regime (see [20]); when unstable, chaotic motion is only confined to the rather thin stochastic layers of the resonances. On the other hand, in the literature it is common to find the opposite scenario, named the Chirikov regime, when the perturbation parameters are large and then an overlap of resonances takes place. Along these lines, we refer to [2] in order to verify that Chirikov, in his well-known review [14] (particularly in its Sec. 7), was mostly interested in the regime of quite confined chaotic motion.

In such a case of restricted chaos ($\mu\varepsilon \ll \varepsilon \ll 1$), taking $I_2 = \omega_2$ irrational, Chirikov's derivations rest on the following computations and assumptions (see [14]):

(i) The variations of H and H_2 are given by

$$\dot{H} = \mu \frac{\partial V}{\partial t}, \quad \dot{H}_2 = I_2 \dot{I}_2 = -\mu \omega_2 \frac{\partial V}{\partial \vartheta_2},$$

where μV is given in (7).

Setting $\vartheta_2(t) \approx \omega_2(t - t_0) + \vartheta_2^0$, with ϑ_2^0 the value of ϑ_2 when $t = t_0$ and $\vartheta_1(t) \approx \vartheta_1^{\text{sx}}(t) = 4 \arctan(\exp(\sqrt{\varepsilon}(t - t_0)))$, i.e., the motion on the separatrix of the guiding resonance is defined in such a way that $\vartheta_1^{\text{sx}} = \pi$ for $t = t_0$ and $\vartheta_1^{\text{sx}}(t) \rightarrow 0 \pmod{2\pi}$ when $t \rightarrow \pm\infty$. The latter is related to the usual definition of the separatrix equation, $\psi^{\text{sx}}(t)$, such that at $t = t_0$ it is $\psi^{\text{sx}} = 0$, through $\vartheta_1^{\text{sx}} = \psi^{\text{sx}} + \pi$.

Thus, neglecting free oscillatory terms in (7), $\sin t$ and $\cos \vartheta_2$ (see, however, Sec. IV), the changes in H and H_2 over a half-period of oscillation of ϑ_1 , $T(|h_1| \ll 1) = \pi/\omega_{\text{sx}}$ given in (5), are

$$\begin{aligned} \Delta H &= \frac{\sqrt{\varepsilon}\mu}{2} A_2\left(\frac{1}{\sqrt{\varepsilon}}\right) \sin t^0, \\ \Delta H_2 &= \frac{\sqrt{\varepsilon}\mu\omega_2}{2} A_2\left(\frac{\omega_2}{\sqrt{\varepsilon}}\right) \cos \vartheta_2^0, \end{aligned} \quad (11)$$

where t^0 is the value of the time $[\text{mod}(2\pi)]$ or phase t when the motion in H_1 crosses the surface $\vartheta_1 = \pi$, $\vartheta_2^0 = \vartheta_2(t^0)$, and

$$A_2(\lambda) = 4\pi\lambda \frac{\exp(\pi\lambda/2)}{\sinh(\pi\lambda)} \quad (12)$$

is the Melnikov-Arnold integral (MAI) of index 2.

In (11) for the changes ΔH , ΔH_2 , the contributions of the MAI of negative arguments were neglected, since it was assumed that $\varepsilon \ll 1$ ($\lambda \gg 1$) and so $A_2(-\lambda) = A_2(\lambda) \exp(-\pi\lambda) \ll A_2(\lambda)$; otherwise, the sum $A_2(\lambda) + A_2(-\lambda)$ should be considered (see below). Indeed, the perturbation (7) is symmetric in $(\vartheta_1 \pm \vartheta_2)$, $(\vartheta_1 \pm t)$ and thus, for instance when moving on the upper branch of the separatrix, $(\vartheta_1 - \vartheta_2)$ leads to $A_2(\lambda)$ while $(\vartheta_1 + \vartheta_2)$ leads to $A_2(-\lambda)$. The opposite occurs when moving on the lower branch of the separatrix.

Notice that $\Delta H = \Delta H_0$ as follows from $\Delta H_1 = -\mu I_1 \partial V / \partial \vartheta_1$, taking $I_1 = I_1^{\text{sx}} = 2\sqrt{\varepsilon} \sin(\vartheta_1^{\text{sx}}/2)$, and using that $\vartheta_1^{\text{sx}} = \psi^{\text{sx}} + \pi$, it is straightforward but tedious to show that $\Delta H_1 = \Delta H - \Delta H_2$ using the recurrence relationship $A_3(\lambda) + A_1(\lambda) = \lambda A_2(\lambda)$; see [14] for details.

(ii) Any significant variation in H is only possible due to large changes in H_2 , since H_1 is bounded to the finite width of the chaotic layer and no significant overlap of the guid-

ing resonance with $\omega_1 = \pm 1$ and other high-order resonances may take place at quite small values of the parameters. Thus defining diffusion coefficients $D_H = \langle [H(t) - H(0)]^2 \rangle / t$ and $D_2 = \langle [H_2(t) - H_2(0)]^2 \rangle / t$, where $\langle \cdot \rangle$ denotes space average, for times large enough, it is expected that $D_H = D_2$ and therefore

$$\langle \sin^2 t^0 \rangle = v^2 \langle \cos^2 \vartheta_2^0 \rangle,$$

where

$$\begin{aligned} v &= \frac{\omega_2 A_2\left(\frac{\omega_2}{\sqrt{\varepsilon}}\right)}{A_2\left(\frac{1}{\sqrt{\varepsilon}}\right)} = \omega_2^2 \frac{\sinh(\pi/\sqrt{\varepsilon})}{\sinh(\omega_2\pi/\sqrt{\varepsilon})} e^{\frac{(\omega_2-1)\pi}{2\sqrt{\varepsilon}}} \\ &\approx \omega_2^2 e^{\frac{(1-\omega_2)\pi}{2\sqrt{\varepsilon}}}, \quad \varepsilon \ll 1, \end{aligned} \quad (13)$$

and in the last approximation the asymptotic value $\sinh x \approx \exp(x)/2$ is used.

It is evident that $v \ll 1$ whenever $\omega_2 > 1$ provided that ε is small enough, but, as discussed in [21], the above approximation for $\omega_2 < 1$ is valid in a narrow interval around $\omega_2 \approx 4\sqrt{\varepsilon}/\pi$ where $v \gg 1$. Indeed, the maximum of v is attained at $\omega_2^0 = 4\sqrt{\varepsilon}/\pi$, and approximating v by a Gaussian around ω_2^0 , the corresponding standard deviation is $\omega_2^0/\sqrt{2}$, so $v \gg 1$ whenever $|\omega_2 - \omega_2^0| \leq \omega_2^0/\sqrt{2}$. Clearly $v \rightarrow 0$ in both limits, $\omega_2 \rightarrow 0, \infty$, and its maximum value at ω_2^0 is $16\pi^{-2} e^{-2\varepsilon} \exp(\pi/(2\sqrt{\varepsilon}))$.

Therefore, it is clear that for $0 < |\omega_2| \neq 1$, both phases t_0 and ϑ_2^0 could not be simultaneously random, in the sense that $\langle \sin^2 t^0 \rangle, \langle \cos^2 \vartheta_2^0 \rangle \sim 1/2$.

(iii) The finite variation of the energy in H_1 over a half-period of oscillation (or a rotation period) near the separatrix of the resonance $\omega_1 = 0$ is given by the difference $\Delta H_1 = \Delta H - \Delta H_2$, so from (11) it follows that

$$\begin{aligned} \Delta H_1 &\equiv H_1' - H_1 = \frac{\sqrt{\varepsilon}\mu}{2} A_2\left(\frac{1}{\sqrt{\varepsilon}}\right) (\sin t^0 - v \cos \vartheta_2^0) \\ &= \hat{W} (\sin t^0 - v \cos \vartheta_2^0). \end{aligned}$$

Introducing the relative energy of H_1 , $w = H_1/\varepsilon$, defining

$$W = \frac{\hat{W}}{\varepsilon} = \frac{\mu}{2\sqrt{\varepsilon}} A_2\left(\frac{1}{\sqrt{\varepsilon}}\right) = \frac{2\pi\mu \exp(\pi/2\sqrt{\varepsilon})}{\varepsilon \sinh(\pi/\sqrt{\varepsilon})}, \quad (14)$$

with $\Delta t_0 \equiv t_0' - t_0 = T_{\text{sx}}$ and if $I_2 \approx \omega_2$ is nearly constant, then $\Delta \vartheta_2^0 = \omega_2 T_{\text{sx}}$.

Denoting with $\tau = t^0$ and $\vartheta_2 = \vartheta_2^0$, the following map arises:

$$\begin{aligned} w' &= w + W [\sin \tau - v \cos \vartheta_2], \quad \tau' = \tau - \frac{1}{\sqrt{\varepsilon}} \ln |w'| + \eta, \\ \vartheta_2' &= \vartheta_2 - \frac{\omega_2}{\sqrt{\varepsilon}} \ln |w'| + \omega_2 \eta, \end{aligned} \quad (15)$$

where $\eta = (\ln 32)/\sqrt{\varepsilon}$.

Chirikov [14] proposed this map not only to describe the chaotic layer around the guiding resonance but also the diffusion along the latter. Indeed, for $\omega_2 > 1$ ($0 < \omega_2 \sim 4\sqrt{\varepsilon}/\pi$) since $v \ll 1$ ($v \gg 1$), on the right-hand side of the equation for w in (15), a dominant term is present. At this order, the map reduces to a whisker mapping, being the largest term (layer resonance in Chirikov's terminology) responsible for the properties of the chaotic layer, such as its width, mean period of motion, and resonances' structure.

For instance, if $v \ll 1$, the width of the layer is given by $W/\sqrt{\varepsilon}$, while if $v \gg 1$ it is $Wv\omega_2/\sqrt{\varepsilon}$, the period of motion being $T(w) \approx \varepsilon^{-1/2} \ln(32\varepsilon/|w|)$ for τ while $T(w) \approx \omega_2\varepsilon^{-1/2} \ln(32\varepsilon/|w|)$ for ϑ_2 .

Thus for large times, it is expected that the successive values of the phase involved in such a dominant term would be correlated (τ for $\omega_2 \gg 1$ and ϑ_2 for $\omega_2 \sim 4\sqrt{\varepsilon}/\pi$), since the map describes the stochastic layer of the guiding resonance whose width is finite.

On the other hand, the successive values of the phase appearing in the smaller term can be assumed to be nearly random, and this perturbing term (the driving resonance according to Chirikov) is responsible for a nearly normal diffusion process along the guiding resonance. In other words, for $0 < \omega_2 \sim 4\sqrt{\varepsilon}/\pi < 1$ it is expected that $\langle \sin^2 \tau \rangle \approx R/2$, $\langle \cos^2 \theta_2 \rangle \ll 1$ while for $\omega_2 > 1$, $\langle \cos^2 \theta_2 \rangle \approx R/2$, $\langle \sin^2 \tau \rangle \ll 1$, where R is the so-called reduction factor (see [14]) that takes into account correlations due to resonances in the stochastic layer that would reduce the diffusion rate. In [14] it is estimated as the relative area of the central part of the layer where the motion is nearly ergodic, i.e., $R \approx 1/4$.

From the above derivations, Chirikov provides an estimate of the timescale for the diffusion along the layer of the guiding resonance. Using the asymptotic expressions for the hyperbolic functions, it reads (see also a discussion given in [18] and references therein)

$$D(\omega_2, \varepsilon, \mu) \sim \begin{cases} \frac{8\pi\omega_2^4\mu^2R}{T_a(\omega_2)} \exp\left(\frac{-\pi|\omega_2|}{\sqrt{\varepsilon}}\right), & |\omega_2| > 1, \\ \frac{8\pi\mu^2R}{T_a(\omega_2)} \exp\left(\frac{-\pi}{\sqrt{\varepsilon}}\right), & 0 < |\omega_2| < 1. \end{cases} \quad (16)$$

Here T_a is the mean period of motion within the chaotic layer of the resonance $\omega_1 = 0$, defined as follows. If $s = w/w_s$, where $w_s \geq |w|$ is the width of the stochastic layer, then

$$T_a = \int_0^1 T(s)ds \approx \lambda \int_0^1 \ln\left(\frac{32}{sw_s}\right)ds,$$

where λ denotes the frequency ratio, i.e., either $1/\sqrt{\varepsilon}$ or $\omega_2/\sqrt{\varepsilon}$ (see the discussion below). It is straightforward to show that

$$T_a = \lambda \ln\left(\frac{32e}{\lambda\tilde{W}}\right), \quad (17)$$

with $e = \exp(1)$ and $\lambda\tilde{W} = w_s$; the latter depends on the value of v , $\lambda = 1/\sqrt{\varepsilon}$, $\tilde{W} \approx W$ for $|\omega_2| > 1$ and thus $w_s = W/\sqrt{\varepsilon} \equiv w_0$, while $\lambda = \omega_2/\sqrt{\varepsilon}$, $\tilde{W} \approx Wv$ for $0 < |\omega_2| < 1$, so $w_s = vw_0\omega_2$.

In terms of the perturbation parameters and ω_2 , using the asymptotic values of the hyperbolic functions in W and v , valid for small ε , the mean period given in (17) reads

$$T_a(\omega_2, \varepsilon, \mu) \approx \begin{cases} \frac{\pi}{2\varepsilon} + \frac{1}{\sqrt{\varepsilon}} \ln\left(\frac{8e\varepsilon^{3/2}}{\pi\mu}\right), & |\omega_2| > 1, \\ \frac{\pi\omega_2}{2\varepsilon} + \frac{1}{\sqrt{\varepsilon}} \ln\left(\frac{8e\varepsilon^{3/2}}{\pi\mu\omega_2^3}\right), & 0 < |\omega_2| < 1. \end{cases} \quad (18)$$

A rough estimation of T_a could be derived using the fact that μ appears in the argument of the logarithmic function in both expressions; so, if $\varepsilon \ll 1$, the dominant terms are $T_a \sim \pi/(2\varepsilon)$ if $|\omega_2| > 1$, and $T_a \sim \pi\omega_2/(2\varepsilon)$ if $0 < |\omega_2| < 1$. Thus,

for $|\omega_2| > 1$, the perturbing phase is τ , while if $0 < |\omega_2| < 1$, it is ϑ_2 with frequencies 1 and ω_2 , respectively. Therefore, from (16) and (18), regarding the diffusion coefficient as a function of μ , it should be $D \sim \mu^p$, $p \approx 2$.

C. Range of validity of the analytical estimates

Chirikov's estimations [14] are valid whenever $\mu \ll 1$ such that the changes in I_2 are small and thus $I_2 \approx \omega_2$ is a plausible approximation in the derivation of ΔH_2 in (11). On the other hand, $\varepsilon \ll 1$ so that $v \gg 1$ or $v \ll 1$ and thus only one term is relevant in the first equation of (15).

To get an order of magnitude of the μ values for which Chirikov's derivations could be applied, we use approximation (9) to determine a theoretical critical value $\mu_{cT}(\varepsilon)$ such that an overlap of the main resonances $\omega_1(I_1) = 0$ and $\omega_1(I_1) = \pm 1$ takes place on the section $\vartheta_1 = \pi$.

This condition reads [see Figs. 2 (right) and 4 (right)]

$$2\sqrt{\varepsilon} + \sqrt{2\varepsilon\mu_{cT}} \approx I_1^r(\varepsilon),$$

leading to

$$\mu_{cT}(\varepsilon) \approx 2\left(1 - \frac{I_1^r}{2\sqrt{\varepsilon}}\right)^2. \quad (19)$$

Figure 2 (left) shows the value of μ_{cT} versus ε given by (19), for the overlap of the resonances $\omega_1(I_1) = 0$ and $\omega_1(I_1) = \pm 1$. Thus the above analytical approximations should be true whenever $\mu \ll \mu_{cT}$.

Regarding the range in ε , it could be required that for the maximum value of v in (13), $16\pi^{-2}e^{-2}\varepsilon \exp(\pi/(2\sqrt{\varepsilon})) \gg 1$, so ε should not be larger than ~ 0.10 , at most.

Certainly, an overlap, or strictly speaking resonance crossings between $\omega_1(I_1) = 0$, $\omega_2(I_2) = 0$, and $\omega_1(I_1) = \pm\omega_2(I_2)$, always exist at any value of ε and $\mu \neq 0$. If $\mu \ll 1$, it is expected that these crossings do not seriously affect the diffusion along the guiding resonance (see, however, Sec. IV).

Note that from this estimation, when $\varepsilon \approx 0.25$ we get $\mu_{cT} \approx 0.17$. However, as the MEGNO¹ contour plot shows for $\vartheta_1 = \pi$, $\vartheta_2 = 0$, $-2 \leq I_1, I_2 \leq 2$ in Fig. 2 (right), the overlap occurs at $\mu \lesssim 0.10$, so actually $\mu_c(\varepsilon) < \mu_{cT}$, as expected. Indeed, if we compare this figure with Fig. 1, several similarities arise. The guiding resonance and its stochastic layer are clearly observed at $I_1 = \pm 1$ as well as the resonances $\omega_1 = \pm 1$ at both sides of the latter, and $\omega_2 = 0$ with their actual half-widths, $\sqrt{2\varepsilon\mu} \approx 0.22$, for the adopted values of the parameters are clearly seen. On the other hand, Fig. 1 shows many high-order resonances appearing close to the stochastic layer of the guiding resonance, while in Fig. 2 (right) all of them are destroyed by overlap [see also Fig. 4 (right)]. In other words, the overlap of high-order resonances leads to a smaller value of μ_c than the theoretical one obtained from the overlap criterion (19) for the first-order resonances.

This figure also reveals that, for the given values of the parameters, an initial ensemble located on the separatrix of the guiding resonance will evolve not only along the chaotic layer of this resonance but on the resonances $\omega_1 = \pm 1$ as well, and

¹See below for a brief description of this fast dynamical indicator.

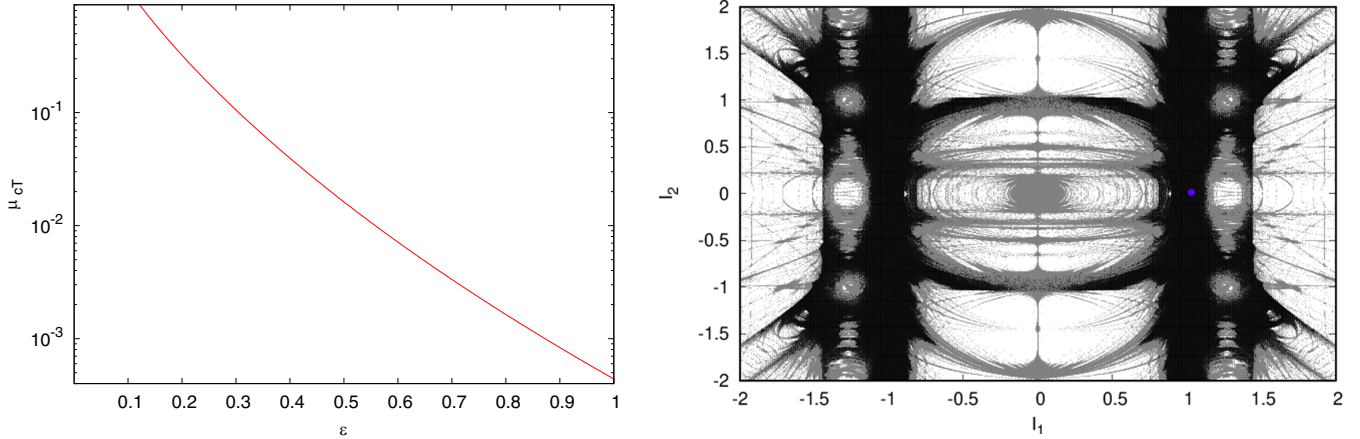


FIG. 2. Left: Critical value of μ (in logarithmic scale) against ε according to (19) for the overlap of the first-order resonances $\omega_1(I_1) = 0$ and $\omega_1(I_1) = \pm 1$. Right: MEGNO contour plot for $\varepsilon = 0.25$, $\mu = 0.10$ showing that for these values of the parameters, the overlap occurs. In the MEGNO contour plot, black indicates $\langle Y \rangle > 65$, gray denotes $2.1 < \langle Y \rangle < 65$, while white means $\langle Y \rangle < 2.1$. The blue dot indicates the location of a given initial ensemble.

therefore the analytical estimates no longer apply. In this scenario, diffusion in both actions would be expected, since the system is not restricted to the stochastic layer of the guiding resonance. Moreover, around $|\omega_2| = 1$, the overlap includes three main resonances: $\omega_1 = 0$, $\omega_1 = \pm 1$, $\omega_2 = \pm \omega_1$.

Therefore, two alternative scenarios must be considered: $0 < |\omega_2| < 1$ and $|\omega_2| > 1$. In fact, for $|\omega_2| \approx 1$ the normal form or the pendulum model for the guiding resonance does not work any longer, while for μ small enough at least a double resonance normal form should be considered. A similar situation would occur if $|\omega_2| \approx 0$, as discussed below.

III. DIFFUSION AND LYAPUNOV TIMESCALES

Herein we discuss two relevant timescales that are always present when the dynamics is chaotic.

A. The diffusion time

A diffusion time can be introduced as the reciprocal of the diffusion rate, $T_D \sim D^{-1}$. However, as was discussed in [18,22], the derivation of T_D from a numerical estimation of D assuming a normal diffusion process does not provide successful results, at least for motion times $\sim 5 \times 10^6$.

Alternatively, T_D can be defined as the required motion time for a given trajectory starting at a given value of I_2 in the chaotic layer of the guiding resonance: $I_1(0) \approx 2\sqrt{\varepsilon}$, $I_2(0) = \omega_2$ arrives at $I_1(t) \approx I_1(0)$, $I_2(t) = I_2(0) \pm \delta$, where $\delta \sim O(1)$. To visualize the instability or diffusion along the stochastic layer of the guiding resonance, Fig. 3 shows for $\varepsilon = 0.25$, $\mu = 0.025$ the evolution of a small random ensemble of size $\xi = 10^{-7}$ and $n_p = 100$ initial conditions centered at $\vartheta_1(0) = \pi$, $\vartheta_2(0) = 0$, $I_1(0) = 2\sqrt{\varepsilon}$, $I_2(0) = \omega_2 = 0.01\sqrt{3}$ for a motion time 4×10^6 on the 3D section $\mathcal{S}_{\vartheta_2=0} = \{(I_1, \vartheta_1, I_2) : |\vartheta_2| < 2 \times 10^{-4}\}$.

For these values of the parameters and motion time, the variation of I_2 is large but bounded: $|I_2(t) - I_2(0)| \lesssim 2$. If instead we take $\mu\varepsilon \ll \varepsilon \ll 1$, the diffusion would be quite restricted over any similar time-span; only in this scenario is

Chirikov's approximation valid (see the discussion given in Sec. IV). Also if $|\omega_2|$ is large, the diffusion is rather confined.

B. The Lyapunov time

The Lyapunov time, T_L , is defined as the reciprocal of the maximum Lyapunov exponent (mLE) of a given trajectory; thus if σ denotes the mLE of an orbit, then $T_L = \sigma^{-1}$. As far as we know, no analytical estimates of σ for this particular system have been reported, not even for small values of the parameters.

Therefore, herein an estimate of the mLE will be provided following the approach given in [15], where it is shown that for a resonance multiplet in a 1.5 dof system, i.e., a pendulum plus a periodic symmetric time-dependent perturbation of fre-

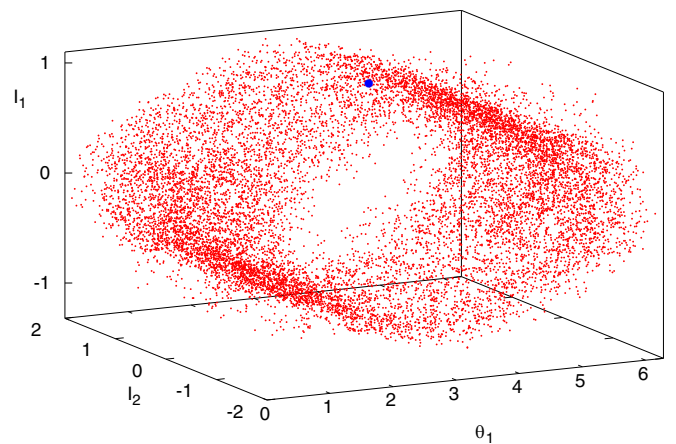


FIG. 3. Observed diffusion during a time interval 4×10^6 for $\varepsilon = 0.25$, $\mu = 0.025$ of a small ensemble (depicted in blue) of $n_p = 100$ initial conditions in the stochastic layer of the guiding resonance where $\vartheta_1(0) = \pi$, $\vartheta_2(0) = 0$, $I_1(0) = 2\sqrt{\varepsilon}$, $I_2(0) = 0.01\sqrt{3}$. The plot is a projection of the full motion on the 3D section $\mathcal{S}_{\vartheta_2=0} = \{(I_1, \vartheta_1, I_2) : |\vartheta_2| < 2 \times 10^{-4}\}$.

quency Ω , the Lyapunov time is given by

$$T_L \approx \frac{1}{\Omega} \frac{T_a(\lambda, \tilde{W})}{\sigma_{sx}}, \quad (20)$$

where σ_{sx} is the mLE of the motion in the stochastic layer of the pendulum system, T_a is the mean period of motion in the layer, and, if the frequency ratio $\lambda \gtrsim 1$, $\lambda \tilde{W} = w_s$ is its width.

Thus, in this particular case, we take σ_{sx} as the mLE of the chaotic layer of the guiding resonance, T_a as the mean period of motion in the layer, given in (17), and Ω as the frequency of the perturbation of the motion in (I_1, ϑ_1) . Moreover, $\lambda = \Omega/\omega_0$, where $\omega_0 = \sqrt{\varepsilon}$ is the small oscillation frequency of the pendulum, and Ω is the frequency of the perturbation, 1 or ω_2 , depending on the value of ω_2 (or v).

In [14,15,23], σ_{sx} is shown to be nearly constant when $\lambda \gtrsim 1$, $\sigma_{sx} \approx C_h \approx 0.80$, called afterwards Chirikov's constant, while in [25] a dependence of σ_{sx} on λ is provided, $\sigma_{sx} \approx 2\lambda C_h/(1+2\lambda)$, that approaches C_h for large λ . Thus (20) reduces to

$$T_L \approx \frac{1+2\lambda}{2\Omega\lambda C_h} T_a(\lambda, \tilde{W}), \quad (21)$$

where, in order to admit not only large values of λ , $A_2(\lambda)$ and $A_2(-\lambda)$ should be considered in both ΔH_1 , ΔH_2 given by (11) and thus in the relative amplitude v , so W given in (14), that defines $\tilde{W} \approx W$ or $\tilde{W} \approx Wv$ if $0 < \omega_2 < 1$ or $\omega_2 > 1$, respectively, should be modified including the contribution of the MAI of negative argument (see [24]). Along these lines, recalling the expressions of $A_2(\lambda)$ and $A_2(-\lambda)$, $\tilde{A}_2(\lambda) \equiv A_2(\lambda) + A_2(-\lambda) = 4\pi\lambda/[\sinh(\pi\lambda/2)]$, W reads

$$W \approx \frac{\mu}{2\sqrt{\varepsilon}} \tilde{A}_2(1/\sqrt{\varepsilon}) = \frac{2\pi\mu}{\varepsilon \sinh(\pi/(2\sqrt{\varepsilon}))}.$$

The perturbation of $H_1(I_1, \vartheta_1)$ comes from two different terms, one involving $\cos(\vartheta_1 \pm t)$ and another one of the form $\sin(\vartheta_1 \pm \vartheta_2)$, both with the same amplitude $\varepsilon\mu/2$ but different frequency.

Assume that $\omega_2 < 1$ but not too small, so $v \gg 1$ and thus the map (15) reduces to

$$w' \approx w - Wv \cos \vartheta_2, \quad \vartheta_2' = \vartheta_2 - \frac{\omega_2}{\sqrt{\varepsilon}} \ln |w'| + \omega_2 \eta.$$

Therefore, just a single term is involved in the perturbation to the separatrix of the pendulum, and it follows that $\Omega = \omega_2$, $\lambda = \omega_2/\sqrt{\varepsilon}$, $T_a = \lambda \ln(32e/(\lambda\tilde{W}))$ with

$$\tilde{W} \approx Wv = \frac{\mu\omega_2}{2\sqrt{\varepsilon}} \tilde{A}_2\left(\frac{\omega_2}{\sqrt{\varepsilon}}\right) = \frac{2\pi\mu\omega_2^2}{\varepsilon \sinh(\pi\omega_2/(2\sqrt{\varepsilon}))},$$

$$\lambda\tilde{W} \approx \frac{2\pi\mu\omega_2^3}{\varepsilon^{3/2} \sinh(\pi\omega_2/(2\sqrt{\varepsilon}))},$$

and thus (21) reduces to

$$T_L \approx \frac{1+2\omega_2/\sqrt{\varepsilon}}{2\omega_2 C_h} \ln\left(\frac{32e}{\lambda\tilde{W}}\right). \quad (22)$$

If $\omega_2 \ll 1$, as is the case for Fig. 3, where $\omega_2 = 0.01\sqrt{3} < 4\sqrt{\varepsilon}/\pi$, as well as if $\omega_2 > 1$, the amplitude v is small, and the map (15) becomes

$$w' \approx w + W \sin \tau, \quad \tau' = \tau - \frac{1}{\sqrt{\varepsilon}} \ln |w'| + \eta,$$

and thus $\tilde{W} \approx W$, $\Omega = 1$, $\lambda = 1/\sqrt{\varepsilon}$. Therefore, in this scenario, T_L given by (21) reads

$$T_L \approx \frac{1+2/\sqrt{\varepsilon}}{2C_h} \ln\left(\frac{32e}{\lambda\tilde{W}}\right),$$

$$\lambda\tilde{W} \approx \frac{\mu}{2\varepsilon} \tilde{A}_2(1/\sqrt{\varepsilon}) = \frac{2\pi\mu}{\varepsilon^{3/2} \sinh(\pi/(2\sqrt{\varepsilon}))}. \quad (23)$$

As a function of μ , T_L in both cases takes a very simple form, $T_L \approx -B(\varepsilon) \ln(\beta(\varepsilon)\mu)$.

These estimations of T_L will be compared with the ones obtained by numerical means. Along these lines, to compute numerically T_L , we take advantage of a fast dynamical indicator, the so-called mean exponential growth factor of nearby orbits (MEGNO) (see [26–28]). The MEGNO, denoted as $\langle Y \rangle$, requires the solution of the variational equations and the usual renormalization of the tangent vector, and it provides an accurate estimate of the mLE of a given trajectory, since $\langle Y \rangle(t) \rightarrow \sigma t/2$, $t \gg 1$ whenever $\sigma > 0$ while $\langle Y \rangle(t) \rightarrow 2$ for quasiperiodic motion. Values of $\langle Y \rangle < 2$ correspond to resonant or stable periodic motion. Therefore, after a certain large enough time-span t , the numerical mLE $\sigma_{\text{num}}(t) = 2\langle Y \rangle(t)/t$ converges to the expected value of the mLE σ .

To be confident of the results, σ_{num} are also derived following Ref. [29], i.e., computing the sum of the renormalized norms of the tangent vector (after a certain number of iterates) and later on dividing it by the total motion time. No relevant differences were observed in all the experiments, but the MEGNO turns out to be much more efficient to perform chaotic contour plots, as we shall see.

We focus then on both timescales T_{inst} and T_L and on any eventual relation between them when this system starts the motion in the stochastic layer of the guiding resonance. Since we are interested in a wide range of values of the parameters, it is expected that the analytical approximations would not work over the full range of ε and μ and thus definitively numerical experiments are required. Certainly, in some ranges of parameter space the theoretical estimates would apply, and we will discuss whether the numerical ones would be represented by the analytical estimates.

Let us mention that the relevant parameter in the Arnold model is μ since the product $\mu\varepsilon$ controls the strength of the coupling between the different degrees of freedom. If $\mu = 0$, as we have already discussed, the system is integrable, and, in this case, the Hamiltonian (3) could be rescaled and shifted so that, after the canonical transformation $t' = \sqrt{\varepsilon}t$, $I_1' = I_1/\sqrt{\varepsilon}$, $H_1' = H_1/\varepsilon + 1$, $\vartheta_1' = \vartheta_1$, the transformed Hamiltonian reads

$$H_1'(I_1', \vartheta_1') = \frac{I_1'^2}{2} + \cos \vartheta_1',$$

independent of ε (see [30]). Therefore, we will focus on the dependence of both timescales, T_D , T_L on μ for particular values of ε .

In all numerical experiments, the integrations were carried out with a Runge-Kutta 7/8th-order integrator, the so-called DOPRI8 routine ([31,32]), with the local tolerance set to 10^{-13} .

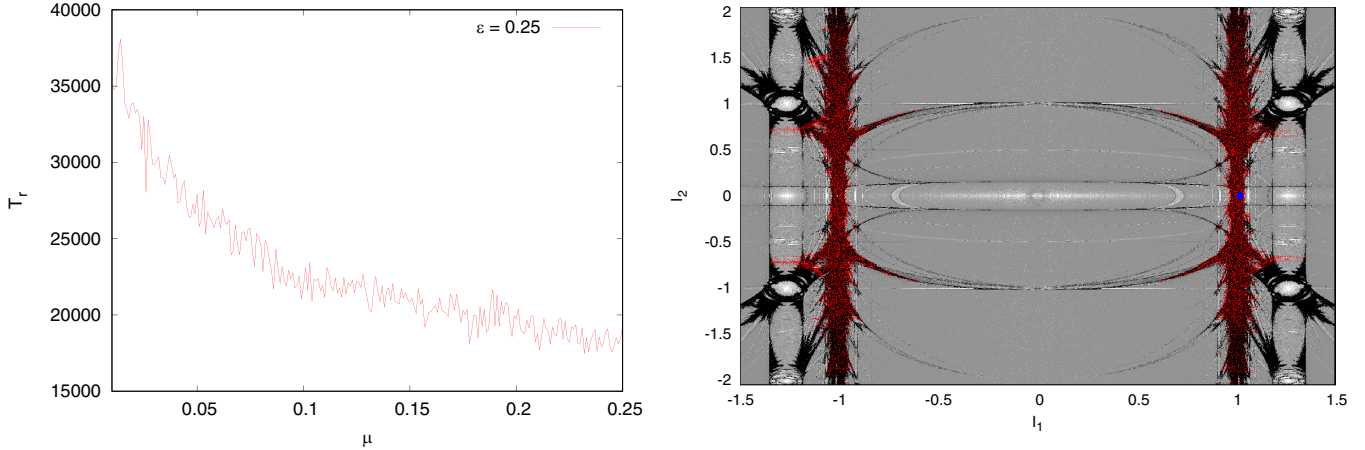


FIG. 4. Left: Recurrence time, T_r , over the section $\mathcal{S}_{\vartheta_1=\pi}^{\vartheta_2=0}$ as a function of μ just for $\varepsilon = 0.25$, $0.01 \leq \mu \leq 0.25$. Right: An initial ensemble (indicated as a blue circle) is followed onto the MEGNO contour plot for $\varepsilon = 0.25$, $\mu = 0.025$; white and light gray denote stable motion, while black indicates strongly chaotic dynamics. The concomitant trajectories for the initial ensemble that intersect the 2D section $\mathcal{S}_{\vartheta_1=\pi}^{\vartheta_2=0}$ are depicted in red.

IV. NUMERICAL RESULTS

As in the experiment presented in Fig. 3, we take a small ensemble of $n_p = 50$ random initial conditions of size $\xi = 10^{-7}$ on the actions for given values of ε and μ with initial conditions $\vartheta_1(0) = \pi$, $\vartheta_2(0) = 0$, $I_1(0) = 2\sqrt{\varepsilon}$, $I_2(0) = \omega_2^0 = 0.01\sqrt{3}$, and the MEGNO is obtained for each one of the n_p initial conditions after $t = 10^5$. Then the average MEGNO over the ensemble, $\langle Y \rangle_e$, is computed and the numerical mLE for the ensemble is obtained as $\sigma_{\text{num}} = 2\langle Y \rangle_e/t$ and thus $T_L = 1/\sigma_{\text{num}}$. Let us recall that the use of ensembles reduces the stickiness effects always present in almost all near-integrable Hamiltonian systems when dealing with finite motion times (see the discussion below in Sec. IV B).

On the other hand, for the same set of initial conditions but $n_p = 100$, the diffusion time, T_D , is computed on the 2D section $\mathcal{S}_{\vartheta_1=\pi}^{\vartheta_2=0} = \{(I_1, I_2) : |\vartheta_1 - \pi| + |\vartheta_2| < 0.01\}$. It is defined as the average time over the n_p trajectories to move along the stochastic layer of the guiding resonance in such a way that on $\mathcal{S}_{\vartheta_1=\pi}^{\vartheta_2=0}$, $|I_2(T_D) - I_2(0)| = \delta \sim O(1)$. Let us mention that the dynamics on $\mathcal{S}_{\vartheta_1=\pi}^{\vartheta_2=0}$ is sensitive to the integration time-step. Indeed, from one side, it is necessary that the recurrence time on the section, T_r , be much smaller than T_D and, on the other side, that the number of intersections of the trajectory with the section be large in order to get smooth average times.

A. Settings and further estimates

Let us start with an illustrative experiment for which we kept the values of n_p , ξ and motion time used to perform Fig. 3, i.e., $n_p = 100$, $\xi = 10^{-7}$, $t = 4 \times 10^6$, and the average recurrence time over the section is much less than 10^5 .

Figure 4 (left) shows the recurrence time as a function of μ just for $\varepsilon = 0.25$ within a wide range, $0.001 < \mu < 0.25$, $T_r < 4 \times 10^4$, and for the larger values of μ it is less than 2×10^4 . The average number of intersections of the trajectory with $\mathcal{S}_{\vartheta_1=\pi}^{\vartheta_2=0}$ is about 1500.

Figure 4 (right) illustrates the diffusion for $\varepsilon = 0.25$ and $\mu = 0.025$ (the same values of the parameters as in Fig. 3)

where the wandering of the actions for the initial ensemble (depicted in blue) is pursued and superimposed on the MEGNO contour plot (for $|I_1| \leq 1.5$, $|I_2| \leq 2$); the red dots correspond to the 100 trajectories that intersect the section $\mathcal{S}_{\vartheta_1=\pi}^{\vartheta_2=0}$. White and light gray colors in the MEGNO contour plot denote stable motion, quite small σ_{num} , while black indicates highly chaotic dynamics, large σ_{num} . As expected, for these values of the parameters, no overlap between the resonances $\omega_1 = 0$ and $\omega_1 = \pm 1$ is present, and the variation of I_2 is large.

According to the results provided in Fig. 4, for the determination of T_D in the dynamics on the section $\mathcal{S}_{\vartheta_1=\pi}^{\vartheta_2=0}$, we adopt $\delta = 0.5$ and focus our studies on the dynamics whenever $|\omega_2| < 1$. Indeed, we adopt $\delta < 1$ in order to avoid the effects of crossings between the guiding resonance and the resonances $\omega_2 = \pm\omega_1$, where the diffusion may spread over both resonances [see Fig. 4 (right)]. However, additional numerical experiments were carried out with $\delta = 0.3$ and 0.7 , which showed that the computed T_D barely changes; just a small shift upwards or downwards with respect to the results for $\delta = 0.5$ is observed.

According to Chirikov [14], when $0 < |\omega_2| < 1$ ($v \gg 1$) the resonances $\omega_1 = \pm\omega_2$ should be mainly responsible for the appearance of the stochastic layer around the separatrix of the guiding resonance as well as for all its properties, while the resonances $\omega_1 = \pm 1$ drive the diffusion along the layer, but if $|\omega_2| > 1$ ($v \ll 1$) these resonances exchange their roles (see, however, the next section).

As mentioned above, for the adopted value of ω_2 in Figs. 3 and 4, $\omega_2 = 0.01\sqrt{3} < 1$, so $v \ll 1$ and thus we should take as the layer resonance $\omega_1 = \pm 1$. Let us discuss this issue in more detail.

For $\varepsilon = 0.25$, $\mu = 0.025$, it follows that $\omega_2 = 0.01\sqrt{3} < \sqrt{2\varepsilon\mu} \approx 0.11$ and thus the initial ensemble lies on the intersection between the stochastic layer of the guiding resonance and the weaker one, $\omega_2 = 0$. It follows then that the term $\sin \vartheta_2$ in μV [see (7)] is slow, and thus at first glance it could not be averaged out. So the approximation $\vartheta_2 \approx \omega_2 t + \vartheta_2^0$ in the computations of ΔH_2 given by (11) is not valid, at least

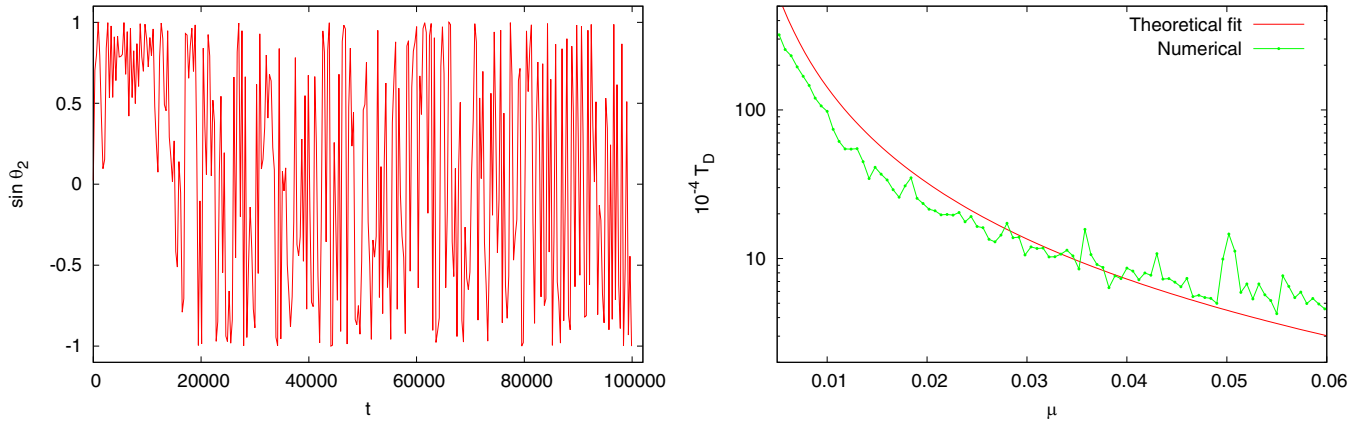


FIG. 5. Left: Evolution of $\sin \vartheta_2$ for $\varepsilon = 0.25$, $\mu = 0.025$; $\vartheta_1(0) = \pi$, $\vartheta_2(0) = 0$, $I_1(0) = 2\sqrt{\varepsilon}$, $I_2(0) = 0.01\sqrt{3}$. Right: Numerical determination of T_D on $\mathcal{S}_{\vartheta_1=\pi}^{\vartheta_2=0}$ and its corresponding theoretical value as $d^2 D^{-1}$ with $d^2 \approx 0.49$, the mean-square distance associated with the wandering of I_2 (see the text for details).

when the motion is confined to the resonance $\omega_2 = 0$, while this fact is irrelevant in the computation of ΔH .

Notice that only when the change in I_2 is small is it possible to approximate $I_2 \approx \omega_2$ as it was done in the computation of ΔH_2 , so the term $\sin \vartheta_2$ would always be resonant. From the experiments presented in Figs. 3 and 4 (left), after a certain motion time, the system leaves the resonance $\omega_2 = 0$, and ϑ_2 will indeed rotate. But this situation is not considered in Chirikov's estimates since the approximation $I_2 \approx \omega_2$ as unperturbed motion is used, but here I_2 exhibits large variations, so the latter approximation does not apply. Actually, as should be expected (and shown in [18]), for the same values of the parameters but taking the initial ensemble in different locations in the stochastic layer, $|\omega_2| < 1$, $|\omega_2| > 1$, and also $|\omega_2| \ll 1$, the diffusion spreads over a quite similar domain regardless of whether ϑ_2 is resonant or not.

Figure 5 (left) shows the evolution of $\sin \vartheta_2$ for the same values of the parameters and initial conditions as in Fig. 4 (left), where it is clearly observed that for motion times less than 2×10^4 this term is resonant.

In conclusion, while the expression for ΔH is correct because it does not depend on (I_2, ϑ_2) , that for ΔH_2 is no longer applicable. Therefore, Chirikov's estimates that involve ω_2 should be revised. Along these lines, notice that if we assume that the driving resonance is $\omega_1 = \pm\omega_2$, then the diffusion coefficient given in (16) is such that $D \rightarrow 0$ while $\omega_2 \rightarrow 0$ as ω_2^4 and then $D^{-1} \approx T_D$ would be extremely large for the considered value of ω_2 . Moreover, from the above numerical experiments, it turns out that it has no sense to distinguish between $|\omega_2| < 1$ and $|\omega_2| > 1$ since I_2 raises up to $|I_2| \approx 2$ when starting at $I_2 = \omega_2 < 1$.

Thus a new experiment is carried out where T_D is computed for $\varepsilon = 0.25$ and $0.005 \leq \mu \leq 0.06$ in the way described above, and also D^{-1} , but instead of using the first line in (16), the latter is modified in order to take into account both contributions of the MAI and the exact expressions of the hyperbolic functions; we obtain

$$D(\omega_2, \varepsilon, \mu) \approx \frac{2\pi^2 \mu^2 \omega_2^4}{T_a(w_s) \sinh^2(\pi \omega_2 / (2\sqrt{\varepsilon}))},$$

where T_a is given by (17) with $w_s = \lambda \tilde{W}$ as in (23). Here we adopt $\omega_2 \approx 0.5$, the value of I_2 when the motion reaches the boundary, $R = 1/4$; and the results are presented in Fig. 5 (right), where the values of D^{-1} , multiplied by a mean-square distance d^2 associated with the wandering of I_2 , should give the diffusion time. The distance d , though it should be ~ 0.5 , is left as a free parameter in order to get the best fit of the numerical values of T_D . Setting $d = 0.7$, fully consistent with the natural value, the analytical estimate $d^2 D^{-1}$ provides the actual order of T_D .

The use of a modified expression for the first line in (16) could be objected if we set $\omega_2 \approx 0.5$ since in such a case the second formula for D applies, for $\omega_2 < 1$ but not too small. Along these lines, if instead the second line in (16) is adopted but also modified in the same direction as above,

$$D(\omega_2, \varepsilon, \mu) \approx \frac{2\pi^2 \mu^2}{T_a(w_s) \sinh^2(\pi / (2\sqrt{\varepsilon}))},$$

with $w_s = \lambda \tilde{W}$ as given in (22), $\omega_2 \approx 0.5$, and $d = 0.7$, the result for the diffusion time is quite similar.

Therefore, if from the numerical computations it follows that $T_D \sim \mu^{-\alpha}$, $\alpha \approx 2$, and $T_L \sim -\ln \mu$, then we may assume that the analytical estimates yield the right dependence of both timescales on μ .

With μ the relevant parameter, we proceed with numerical experiments for different sets of parameter values, consisting of a few values of ε and varying μ in a short-step way within a given interval. Along these lines, three series of experiments are performed.

(I) First, we take $\varepsilon \in \mathcal{E}_1 = \{0.10, 0.15, 0.20, 0.25, 0.30\}$, $\mu \in \mathcal{M}_1 = \{0.001 \leq \mu < \mu_0\}$ with $\delta\mu = 0.0006$, where $\mu_0 = \min\{0.1, 0.5\mu_{cT}(\varepsilon)\}$. Thus, the simulations will end at different values of μ if $\mu_0 < 0.1$, for instance if $\varepsilon = 0.30$, $\mu_0 \approx 0.051$. The integration parameters are $t = 10^5$, $\delta t = 1$ for the determination of T_L while $t = 4 \times 10^6$, $\delta t = 0.05$ in the case of T_D .

The choice of the parameters is such that in the domain $|I_2(t) - I_2(0)| < 1$ no significant overlap nor crossing of resonances occurs, and thus it is reasonable to expect that the analytical estimates would roughly apply, i.e., $T_D \sim 1/\mu^p$

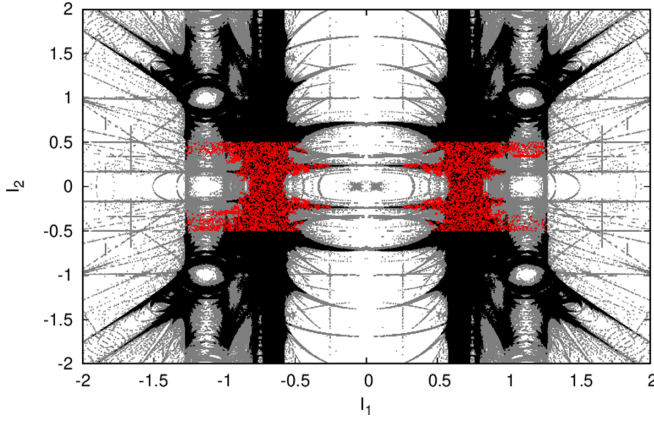


FIG. 6. MEGNO contour plot for $\varepsilon = \mu = 0.12$, where black indicates $\langle Y \rangle > 35$, gray indicates $2.1 < \langle Y \rangle < 35$, and white indicates $\langle Y \rangle < 2.1$. The evolution of the initial ensemble is depicted in red only for $|I_2 - I_2(0)| \leq 0.5$.

with $p \approx 2$ and $T_L \sim -\ln \mu$ should be expected. While only for $\varepsilon \leq 0.10$ is it $v \gg 1$ as discussed above, we expect that up to $\varepsilon \approx 0.25$ the theoretical formulation would apply.

(II) Second, we set $\mu = \varepsilon$ for $\varepsilon \in \mathcal{E}_2 = \{0.001 \leq \varepsilon < \varepsilon_0 < \varepsilon_{cT}\}$ with $\delta\varepsilon = 0.001$. Here ε_{cT} is the theoretical critical value of ε for the existence of an overlap of the guiding resonance with resonances $\omega_1 = \pm 1$. The latter, proceeding in a similar fashion as we have already done for μ_{cT} in (19), should satisfy the equation

$$\eta^2 + 2\sqrt{2}\eta = 32 \exp(-2\pi\eta), \quad \eta = \sqrt{\varepsilon_c},$$

whose numerical solution is $\varepsilon_{cT} \approx 0.23$, so we adopt $\varepsilon_0 \leq 0.18$ in order to avoid any significant overlap. The integration parameters are similar to those of (I) but $t = 5 \times 10^6$ for the determination of T_D .

According to [33], when both parameters are not independent of each other, the estimates of the splitting of separatrices (about $2\tilde{W}$ in this formulation) given by the direct application of the MAI no longer apply, and in that work the case of $\mu = \varepsilon$ is largely investigated by a rigorous analytical approach. Along these lines, numerical estimations of the splitting are given for the perturbation parameter $\eta^2 \equiv \varepsilon = \mu$, ranging from $\eta = 0.02$ up to 0.44, similar to $\varepsilon \in \mathcal{E}_2$. Unfortunately, no analytical estimates for the diffusion coefficient arise in this scenario.

Figure 6 shows the structure of action space on $\mathcal{S}_{\vartheta_1=\pi}^{\vartheta_2=0}$ for $\varepsilon = \mu = 0.12$ as well as the intersections of $n_p = 100$ trajectories with this section whenever $|I_2(t) - I_2(0)| \leq 0.5$. Although the guiding resonance and resonances $\omega_1 = \pm 1$ are not in overlap, there is a path from the stochastic layer of $\omega_1 = 0$ to the domain of resonance $\omega_1 = \pm 1$ through the layers of the resonances $\omega_1 = \pm\omega_2$ and $\omega_2 = 0$; therefore, the diffusion is comparable in both actions.

(III) Third, let $\varepsilon \in \mathcal{E}_3 = \{0.25, 0.30, 0.35, 0.40, 0.45, 0.50\}$, $\mu \in \mathcal{M}_2 = \{0.1 \leq \mu < 0.25\}$ with $\delta\mu = 0.001$. The integration parameters are taken similar to those of (I). This choice of the parameters is such that an overlap of resonances $\omega_1 = 0$ and $\omega_1 = \pm 1$ takes place and thus the scenario is quite far from that given by Chirikov's assumptions.

B. Results

In this section, the main results of the series of experiments are presented and discussed.

1. Experiment I

Figure 7 (left) presents the computed T_D versus μ , $0.001 \leq \mu \leq 0.1$ whenever $\mu_0 \geq 0.1$ for the five values of ε considered. For the smaller values of both parameters, the trajectories do not cross the boundary $|I_2 - I_2(0)| = 0.5$ as the plateau at $T_D = 4 \times 10^6$ reveals. Note that for the two largest values of ε , $\mu_c < 0.1$ for instance, at $\varepsilon = 0.30$ one has $\mu_c \approx 0.11$, so results for $\mu < 0.055$ are presented.

The diffusion time presents a mild dependence with ε ; the latter parameter seems to play the role of a scale factor. A least-squares fit (LSF) of the power law

$$10^{-4}T_D(\varepsilon, \mu) = \frac{A_1(\varepsilon)}{\mu^{\alpha_1(\varepsilon)}}, \quad (24)$$

where, according to Chirikov's estimate, one may expect $\alpha_1 \sim 2$, leads to the values of A_1 and α_1 given in Table I. The corresponding fit for $\varepsilon = 0.15$ is drawn in Fig. 7 (left) as a solid black curve.

Notice that in any case $T_D \approx A_1(\varepsilon)\mu^{-1.6}$, where A_1 decreases with ε , consistent with the analytical approach. The values of the coefficients in Table I depend on the considered range in μ for the LSF, in particular the initial one. For instance, for $\varepsilon = 0.10$ the fit starts at $\mu = 0.024$ since for smaller values of μ , T_D is almost constant.

Figure 7 (right) displays the corresponding results for T_L versus μ , $0.001 \leq \mu \leq 0.1$ using the same color pattern for the different ε values as in the figure at the left. For small ε and μ a nearly constant value of T_L is observed, however large fluctuations are present up to $\mu \lesssim 0.05$. This is a curious behavior similar to that reported in [16] when dealing with the $T_D - T_L$ relationship in a 4D symplectic map derived on a section similar to $\mathcal{S}_{\vartheta_1=\pi}^{\vartheta_2=0}$ for small values of the perturbation parameters.

Along these lines, new experiments are carried out for $\varepsilon = 0.10, 0.15$, and $0.001 \leq \mu \leq 0.05$, where the Lyapunov time is computed for time intervals up to 10^6 for the same ensemble of $n_p = 50$ nearby initial conditions. The results, shown in Fig. 8 (left), do not present significant differences with respect to those displayed in Fig. 7 (right). In fact for $\varepsilon = 0.10$ and $t = 10^6$, T_L takes larger values than when it is computed at $t = 10^5$ in the full range of μ , while the opposite occurs for $\varepsilon = 0.15$ up to $\mu \approx 0.03$. For larger values of μ the results are quite similar.

On the other hand, it could be argued that the use of an ensemble would lead to this particular behavior of T_L , since maybe several trajectories in the ensemble could suffer stickiness producing then an artificial enlargement of the values of the average Lyapunov time. Thus T_L is computed now for $n_p = 1$ and just for $\varepsilon = 0.10$, also over a time-span of 10^6 , and the results are presented in Fig. 8 (center), where it is clearly observed that the fluctuations in T_L are quite large, precisely due to stickiness. Indeed, for $\varepsilon = 0.10$, $0.001 \leq \mu \leq 0.05$ with $\Delta\mu = 0.0006$ and $t = 10^6$, the distribution of T_L for the $n_p = 50$ initial conditions in the ensemble for each μ is presented in Fig. 8 (right), where the nearly 4100 values of the

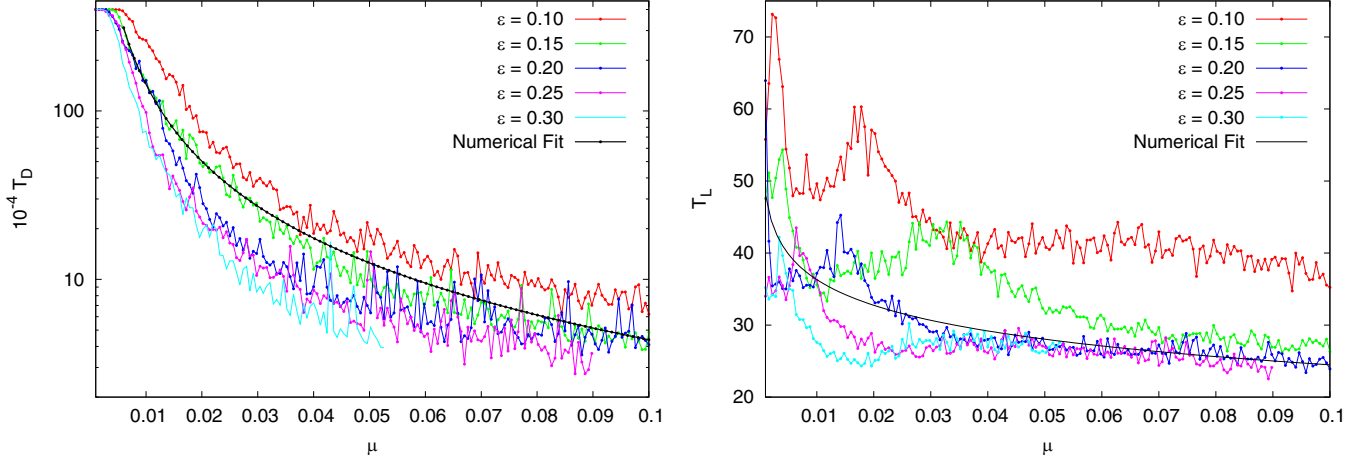


FIG. 7. T_D computed on $\mathcal{S}_{\vartheta_1=\pi}^{\vartheta_2=0}$ and T_L vs μ ; different colors indicate the values of ε . The black full lines in the plots correspond to particular numerical fits (see the text for details).

Lyapunov time are binned in 150 intervals. If some trajectory behaves as regular, it should lead, for the computed motion time, to $T_L \sim 10^6$, while the largest one, just one value, is about 10^3 , so all trajectories are chaotic and those with large T_L are subject to stickiness that influences the average T_L over the ensemble.

Just for comparison, in Fig. 8 (center), the theoretical Lyapunov time is included, actually $1.45T_L$ with T_L given by (23). If instead (22) is adopted for T_L , with $\omega_2 \approx 0.5$, no significant differences are observed.

Figure 9 shows the evolution of the initial ensemble of $n_p = 50$ initial conditions up to the motion time 10^6 for $\varepsilon = 0.10$, $\mu = 0.015$ on $\mathcal{S}_{\vartheta_1=\pi}^{\vartheta_2=0}$ where a contour plot of the MEGNO is included for these values of the parameters. It becomes clear that the trajectories spend most of the time on the stochastic layer close to $|I_2| \leq 0.2$; also some iterates appear in the connection between the guiding resonance with resonances $\omega_1 = \pm\omega_2$ where the diffusion is much slower. This fact could explain the comparatively large value of the average T_L computed at $t = 10^6$. However, this particular behavior of the Lyapunov time for $\mu \leq 0.03$ and small ε requires further theoretical studies.

According to (23), a logarithmic relationship between T_L and μ is proposed,

$$T_L(\varepsilon, \mu) = -B_1(\varepsilon) \ln(\beta_1(\varepsilon)\mu), \quad (25)$$

where the values of B_1 , β_1 are given in Table I; the fit for $\varepsilon = 0.20$ is depicted in Fig. 7 (right) as a black curve. For this value of ε , T_L given by (23) leads to $T_L \approx -3.42 \ln(0.048\mu)$, which provides a similar order than that obtained by fitting

the data. However, as expected, the errors in the parameters are somewhat larger, in particular in β_1 .

From (24) and (25) it follows that

$$10^{-4}T_D \approx C_1(\varepsilon) \exp(\gamma_{1\varepsilon}T_L), \quad (26)$$

with $\gamma_{1\varepsilon} \approx \alpha_1/B_1$, where the expected values of this factor are given in Table I.

Within the irregularities of T_L , the fit (25), as well as (23), seem to be acceptable. Both provide the order of T_L . Notice that for $\varepsilon = 0.30$ no values of $0.01 \leq \mu \leq 0.05$ are given, since T_L is almost constant at $0.01 \leq \mu \leq 0.05$. Using again (23), the corresponding values should be $B_1 \approx 2.91$, $\beta_1 \approx 0.05$.

Considering T_D against T_L , the latter restricted to $22 < T_L < 40$ in order to somewhat reduce its irregular behavior, a LSF for $\varepsilon = 0.15$ leads to $\gamma_{1\varepsilon} \approx 0.17$ while for $\varepsilon = 0.20, 0.25$ we get $\gamma_{1\varepsilon} \approx 0.19$. Clearly for $\varepsilon = 0.10, 0.30$ it has no sense to perform this numerical fit. Though the numerical values of $\gamma_{1\varepsilon}$ are somewhat smaller than α_1/B_1 , they agree in the order. Figure 10 shows a LSF for all the values ($\varepsilon = 0.15, 0.20, 0.25$). The fit is drawn by the solid green line, taking $\gamma_{1\varepsilon} \approx 0.177 \pm 0.015$ and $C_1 \approx 0.112 \pm 0.061$, and for the best fit we adopt $C_1 \approx 0.06$ due to the uncertainty in the estimation of this parameter.

The results obtained in this series of experiments, where no significant overlap of first-order resonances is expected, are consistent with the analytical estimates for both T_D and T_L .

2. Experiment II

Here, as mentioned, $\varepsilon = \mu$ is considered, thus a single result for T_D and T_L against μ is shown. Recall that the range

TABLE I. Values of the parameters A , α , B , and β obtained by a LSF of $10^{-4}T_D$.

ε	A_1	α_1	B_1	β_1	α_1/B_1
0.10	0.170 ± 0.018	1.54 ± 0.03	6.435 ± 0.29	0.0277 ± 0.008	0.239 ± 0.015
0.15	0.133 ± 0.008	1.53 ± 0.02	5.779 ± 0.30	0.0714 ± 0.022	0.265 ± 0.017
0.20	0.043 ± 0.006	1.73 ± 0.03	5.138 ± 0.22	0.0853 ± 0.021	0.337 ± 0.007
0.25	0.038 ± 0.005	1.66 ± 0.03	3.431 ± 0.19	0.0090 ± 0.004	0.483 ± 0.036
0.30	0.019 ± 0.004	1.78 ± 0.04			

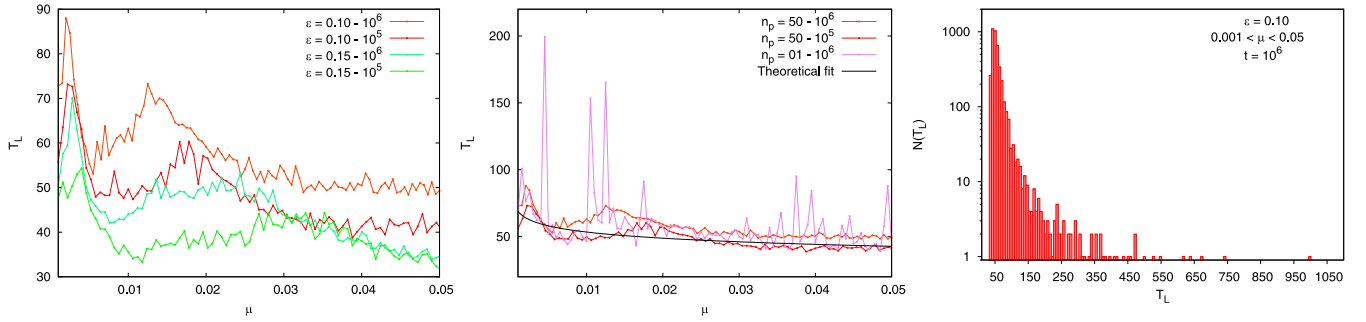


FIG. 8. Left: T_L for $\varepsilon = 0.10, 0.15$ computed up to $t = 10^6$ for $n_p = 50$, $\xi = 10^{-7}$ and the same initial conditions as in Fig. 7 (right). T_L up to $t = 10^5$ for the same values of ε are also included for comparison. Center: similar to the figure at the left but just for $\varepsilon = 0.10$ and taking $n_p = 1$ instead of $n_p = 50$. Also T_L for $n_p = 50$ and $t = 10^5-10^6$ are included. The theoretical expected value given in (23) multiplied by 1.45 is depicted in black. Right: Distribution of T_L (in logarithmic scale) at $\varepsilon = 0.10$ and $0.001 \leq \mu \leq 0.05$ for the $n_p = 50$ initial conditions in the ensemble for each value of μ .

of μ is such that no significant overlap of resonances occurs. The results are shown in Fig. 11 (left and center), where T_D decreases with μ in a nearly exponential way. Notice that T_D , for $\mu < 0.07$, is close to the integration time as the cusp reveals; these values should be ignored since the diffusion time should increase as $\mu \rightarrow 0$. On the other hand, except in a very narrow interval of small values of μ , T_L decreases monotonically with the perturbation parameter as a power law. Note that in this case, if we approximate T_L with (23), $\mu = \varepsilon$ should be considered and the dependence of the Lyapunov time on the perturbation parameter is no longer logarithmic.

Then a LSF for both timescales of the form

$$10^{-4}T_D = A_2 \exp\left(\frac{1}{\mu^{\alpha_2}}\right), \quad T_L = \frac{B_2}{\mu^{\beta_2}} \quad (27)$$

leads to $A_2 \approx 2.24 \pm 1.55$, $\alpha_2 \approx 2.5 \pm 0.155$; $B_2 \approx 3 \pm 0.29$, $\beta_2 \approx 1.084 \pm 0.023$. Both fits are drawn with a solid green curve in Fig. 11 (left and center), where also (23) for the theoretical estimation of T_L with $\mu = \varepsilon$ multiplied by 1.25 is plotted in black. Notice that again, in this particular case, the estimation of T_L provides the right order of the numerical-experimental values, while the laws given in (27)

are in good agreement with the computed values of T_D and T_L .

From (27) it follows that a relationship between T_D and T_L should be of the form

$$10^{-4}T_D = C_2 \exp\left(\frac{T_L}{T_0}\right)^{\gamma_2}, \quad (28)$$

where $\gamma_2 \approx \alpha_2/\beta_2 \approx 2.30 \pm 0.19$ and $T_0 \approx B^{\gamma_2} \approx 30$, within the errors. Along these lines, a LSF by (28) for $20 \leq T_L \leq 60$, i.e., the values of T_D , T_L for $\mu > 0.06$, provides $C_2 \approx 1.55 \pm 0.159$, $\gamma_2 \approx 2.26 \pm 0.04$, very close to the expected ones. This is shown in Fig. 11 (right), where the law (28) is depicted in green, revealing a good accordance between the computed values with the expected relationship between both timescales.

Equation (28) may look similar to the parametric $T_D - T_L$ relation for the standard map discussed in the Introduction, but there are important differences. This underlines the fact that the parametric relationships $T_D - T_L$, contrary to the generic ones, may have rather varied analytical forms.

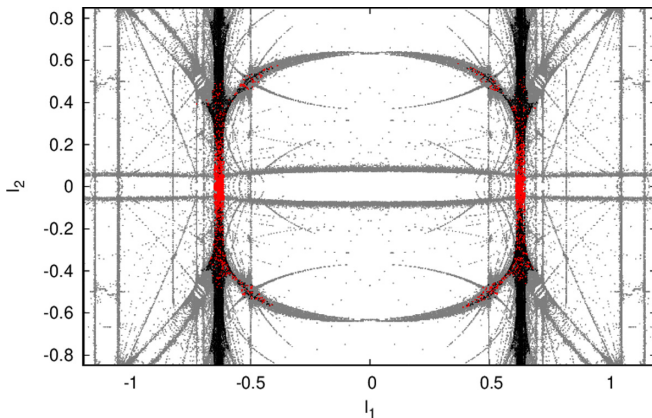


FIG. 9. MEGNO contour plot in (I_1, I_2) space for $\varepsilon = 0.10$, $\mu = 0.015$ and the evolution of an ensemble of $n_p = 50$ initial conditions at the separatrix of the guiding resonance and $\omega_2 = 0.01\sqrt{3}$ on $S_{\vartheta_1=\pi}^{\vartheta_2=0}$. Black and gray denote strong and mild chaos, respectively, while white indicates stable motion.

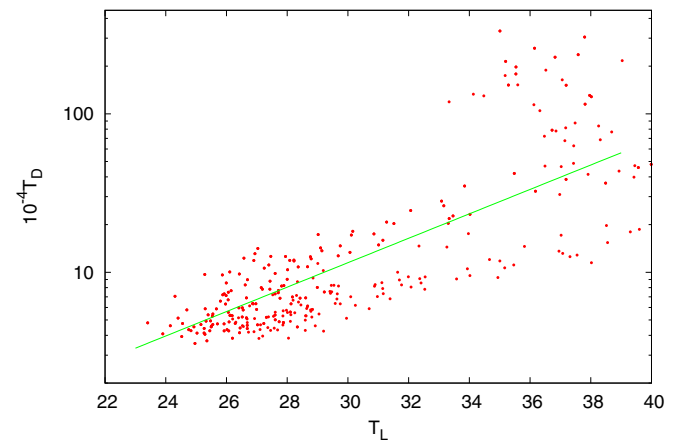


FIG. 10. $10^{-4}T_D$ (in logarithmic scale) vs T_L for $\varepsilon = 0.15, 0.20, 0.25$ and $22 < T_L < 40$. The green line corresponds to the fit (26) for all the data with $\gamma_1 \approx 0.18$ and C_1 taken as the half-value obtained by LSF since its uncertainty is large, $C_1 \approx 0.06$.

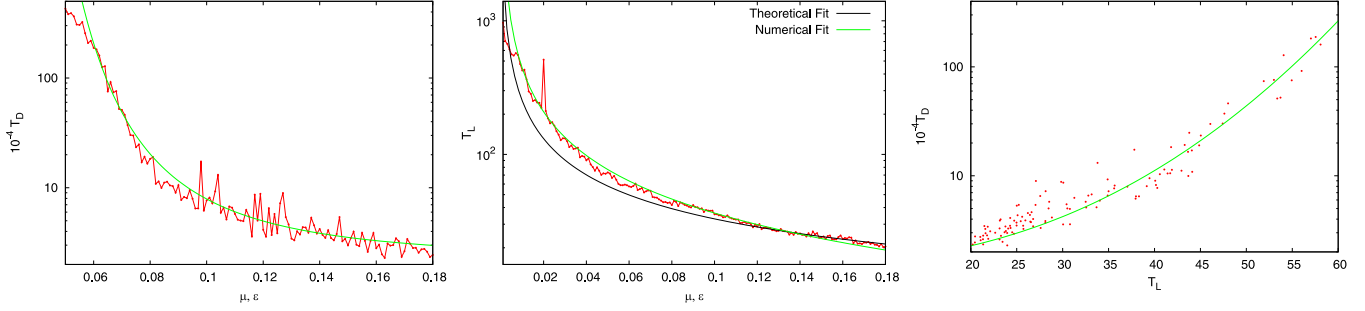


FIG. 11. T_D (in units of 10^4) and T_L as a function of $\mu = \varepsilon$ and T_D against T_L . The green curve in the three plots represents a LSF of the data, while the black one in the central panel corresponds to the theoretical estimation of T_L by means of (23) (see the text for details).

3. Experiment III

Here we deal with the scenario in which $\mu > \mu_c(\varepsilon)$ so no analytical estimate applies. The following values of the parameters are considered: $\varepsilon = 0.25, 0.30, 0.35, 0.40, 0.45$, $0.1 \leq \mu \leq 0.25$, and, according to Fig. 2 (left), when $\varepsilon = 0.25$, $\mu_c \approx 0.1$.

Similar experiments to those discussed before are carried out for both timescales. The results for T_D and T_L are given in Fig. 12.

Notice that while T_D seems to be nearly independent of ε , T_L reveals that this parameter plays the role of a scale factor. In both cases, only a power law for the timescale with μ works; any attempt to fit T_L with a logarithmic dependence on μ (as in Experiment I) fails. Thus the following power laws are fitted:

$$10^{-4}T_D = \frac{A_3(\varepsilon)}{\mu^{\alpha_3(\varepsilon)}}, \quad T_L = \frac{B_3(\varepsilon)}{\mu^{\beta_3(\varepsilon)}}, \quad 10^{-4}T_D = C_3(\varepsilon)T_L^{\gamma_3\varepsilon}. \quad (29)$$

The values of all the parameters are provided in Table II, where the ratio $\alpha_3/\beta_3 \approx \gamma_3\varepsilon$ is included. It is interesting that all the parameters involved in the above fits vary in narrow intervals; in particular, α_3/β_3 is close to 1. In both panels, the fit corresponding to $\varepsilon = 0.35$ is included as a black solid curve.

Figure 13 (left) presents the relation $T_D - T_L$ for this range of parameters, where it becomes evident that a correlation

exists between the timescales. The LSF of $10^{-4}T_D = C_3(\varepsilon)T_L^{\gamma_3\varepsilon}$, after removing the large fluctuations observed at $\varepsilon = 0.25$, leads to the values of C_3, γ_3 given in Table II. Recall that in any case, γ_3 is very close to that of α_3/β_3 . Taking the relation $T_D - T_L$ for all ε to fit by a single power law, it follows that $C_3 = 0.867 \pm 0.076$, $\gamma_3 = 0.46 \pm 0.032$ as Fig. 13 (right) shows, and this power-law fit is included in blue. However, the values of T_D still present fluctuations that introduce noise to the actual correlation parameters, so we include a second fit with $C_3 \approx 0.346$, $\gamma_3 \approx 0.824$, i.e., the values corresponding to $\varepsilon = 0.40$, and the fit is drawn in the figure in black. This second fit also represents well the correlation between both timescales.

This set of experiments, for large values of the parameters, reveals that both timescales obey a power law with μ , where the exponent is in the range 0.3–0.5, and at all ε the exponents are quite similar. These results do not yet allow any analytical derivation.

V. FINAL REMARKS

In this work, it is shown that in the Arnold model, when the perturbation parameters are relatively small, the numerical results concerning T_D and T_L are consistent with the analytical estimates given by [14,15] for the diffusion time and the Lyapunov

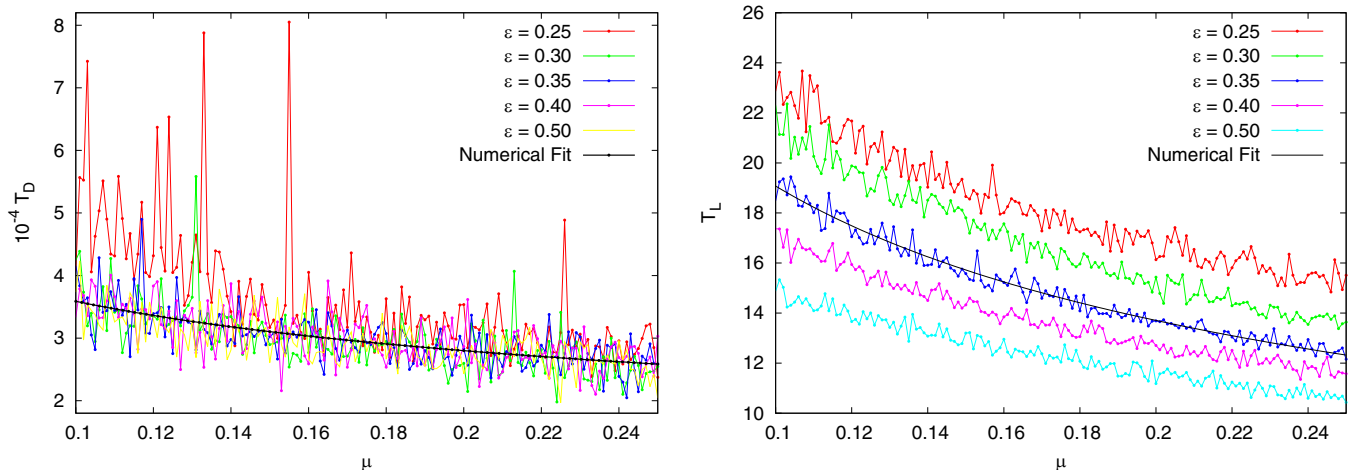


FIG. 12. Left: T_D (in units of 10^4) and T_L as a function of μ , where different colors indicate the corresponding ε values. The black curves represent a LSF of the data for particular values of ε (see the text for details).

TABLE II. Values of the parameters A_3 , α_3 , B_3 , β_3 , C_3 , γ_3 obtained by a LSF of $10^{-4}T_D$ for all values of μ , except for $\varepsilon = 0.25$, where $\mu > 0.14$ and T_L , also for all values of μ .

ε	A_3	α_3	B_3	β_3	α_3/β_3	C_3	γ_3
0.25	1.447 ± 0.294	0.482 ± 0.123	7.983 ± 0.116	0.459 ± 0.008	1.050 ± 0.286	0.149 ± 0.115	1.083 ± 0.274
0.30	1.400 ± 0.098	0.416 ± 0.038	6.710 ± 0.083	0.508 ± 0.007	0.818 ± 0.086	0.320 ± 0.068	0.790 ± 0.075
0.35	1.574 ± 0.091	0.358 ± 0.031	6.360 ± 0.074	0.477 ± 0.006	0.750 ± 0.074	0.425 ± 0.076	0.721 ± 0.066
0.40	1.586 ± 0.095	0.357 ± 0.032	6.426 ± 0.063	0.424 ± 0.005	0.842 ± 0.085	0.346 ± 0.069	0.824 ± 0.076
0.50	1.597 ± 0.089	0.338 ± 0.030	6.387 ± 0.069	0.369 ± 0.006	0.916 ± 0.096	0.335 ± 0.068	0.861 ± 0.080

punov time, respectively. The estimations of T_L , according to [15] and following Chirikov's idea of the existence of a layer resonance, are in agreement with the numerical determinations whenever no significant overlap of first-order resonances occurs.

When ε, μ are both not too small, the estimate for T_D is not clear, since the determination of ΔH_2 does not hold, and therefore it seems irrelevant to distinguish between $|\omega_2| < 1$ or $|\omega_2| > 1$. In any case, we succeed in getting the right order of T_D after adopting for ω_2 the corresponding value at the boundary of the motion.

The numerical outcomes show that, indeed, $T_D \sim \mu^{-\alpha}$ with $\alpha \sim -2$ while $T_L \sim \ln \mu$ as predicted by the theoretical estimates. Thus an exponential relationship between the computed values T_D and T_L arises, as $T_D \sim \exp(T_L)$.

In the particular case of $\mu = \varepsilon$ ($\varepsilon < \varepsilon_{cT}$), the theoretical estimate of T_L agrees with the numerical one, but this is not true for T_D . While this aspect is not completely clear, it seems that it could be related to the fact that, as discussed in [33], a direct application of the MAI to measure the splitting of separatrices does not apply any longer, and thus the estimations of ΔH , ΔH_1 , ΔH_2 , where the MAI are straightforwardly calculated for the first-order resonances, are no longer valid. In [33], a detailed discussion about the use of an averaging technique before applying the Melnikov method is given, and it is shown that this is the right procedure. Along these lines, the full splitting is looked for when different

(high-order) harmonics in the perturbation play a relevant role.

In this specific numerical experiment (with $\mu = \varepsilon$), we found that T_D follows an exponential relationship with μ as $\sim \exp(1/\mu^{2.5})$ while T_L behaves as $\sim \mu^{-1}$ and therefore a $T_D - T_L$ relationship like $T_D \sim \exp(T_L^\gamma)$ applies, with $\gamma \sim 0.3$.

When both parameters are large, such that no analytical estimates apply, it is found that both timescales follow a similar power law with μ as $\sim \mu^{-0.4}$ and therefore also a power law applies for the relation $T_D - T_L$; $T_D \sim T_L^\gamma$, with $\gamma \sim 1$.

These results show that even in this particular model where a continuous family of hyperbolic tori along the guiding resonance exists, the functional relationship $T_D - T_L$ depends on the strength of the perturbation, i.e., on the global dynamics of the system for the given values of ε and μ . Along these lines, it is not expected that the obtained results between both timescales would apply in a more general case.

Regarding Chirikov's approach to the diffusion rate, the estimate provides the right order whenever (i) μ is small enough such that the change in I_2 is quite small, i.e., the diffusion is slow; and (ii) the relative amplitude v is small or quite large. The latter condition restricts the values of $\varepsilon \lesssim 0.10$ whenever $\omega_2 \sim 1.27\sqrt{\varepsilon} \lesssim 1$, while if ω_2 is large, v is always small even for $\varepsilon \lesssim 0.25$ or larger.

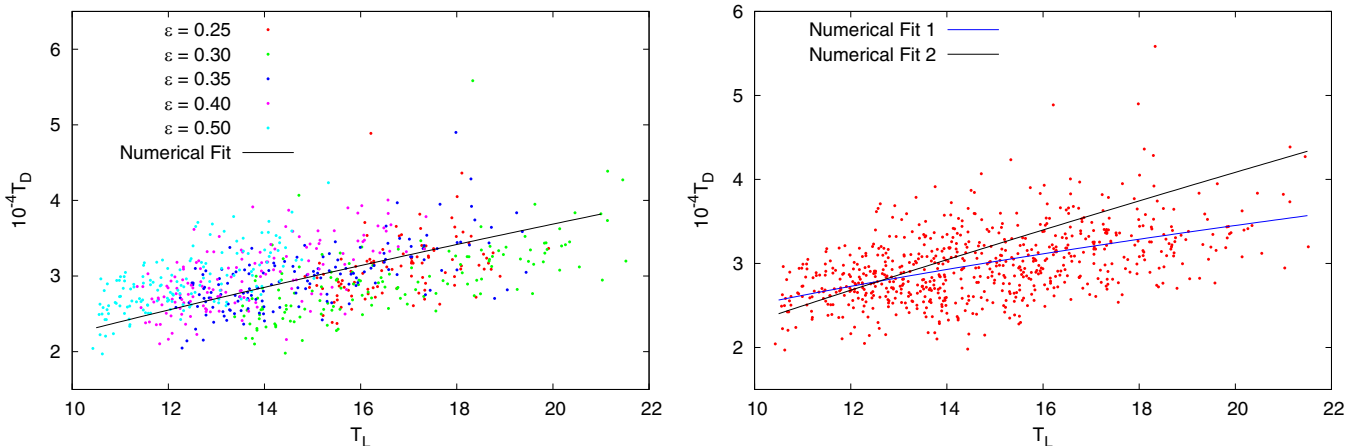


FIG. 13. Left: T_D (in units of 10^4) vs T_L ; different colors indicate the corresponding ε values. The black curve in the figure on the left is the fit for $\varepsilon = 0.35$, and that on the right encompasses the whole data. The two numerical fits are included, one with $C_3 \approx 0.874$, $\gamma_3 \approx 0.46$ in blue, while the black one is for $C_3 \approx 0.346$, $\gamma_3 \approx 0.824$ (see the text for details).

ACKNOWLEDGMENTS

The authors are most thankful to the referees for their valuable suggestions and comments, which have allowed us to improve the manuscript. P.M.C. and C.M.G. were supported by grants from Consejo Nacional de Investigaciones Cientí-

ficas y Técnicas de la República Argentina (CONICET), the Universidad Nacional de La Plata and Instituto de Astrofísica de La Plata. I.I.S. was supported by the Russian Science Foundation (Project No. 22-22-00046).

The authors declare that they have no conflict of interest.

-
- [1] F. Cachucho, P. M. Cincotta, and S. Ferraz-Mello, Chirikov diffusion in the asteroidal three-body resonance (5, -2, -2), *Celest. Mech. Dyn. Astron.* **108**, 35 (2010).
- [2] P. M. Cincotta, C. Efthymiopoulos, C. M. Giordano, and M. F. Mestre, Chirikov and Nekhoroshev diffusion estimates: Bridging the two sides of the river, *Physica D* **266**, 49 (2014).
- [3] C. Efthymiopoulos and M. Harsoula, The speed of Arnold diffusion, *Physica D* **251**, 19 (2013).
- [4] C. Froeschlé, M. Guzzo, and E. Lega, Local and global diffusion along resonant lines in discrete quasi-integrable dynamical systems, *Celest. Mech. Dyn. Astron.* **92**, 243 (2005).
- [5] C. Froeschlé, E. Lega, and M. Guzzo, Analysis of the chaotic behaviour of orbits diffusing along the Arnold web, *Celest. Mech. Dyn. Astron.* **95**, 141 (2006).
- [6] M. Guzzo, E. Lega, and C. Froeschlé, First numerical evidence of global Arnold diffusion in quasi-integrable systems, *Discrete Contin. Dyn. Syst. B* **5**, 687 (2005).
- [7] E. Lega and C. Froeschlé, Guzzo, Diffusion in Hamiltonian quasi-integrable systems, *Lect. Notes Phys.* **729**, 29 (2008).
- [8] E. Lega, M. Guzzo, and C. Froeschlé, Detection of Arnold diffusion in Hamiltonian systems, *Physica D* **182**, 179 (2003).
- [9] J. G. Martí, P. M. Cincotta, and C. Beaugé, Chaotic diffusion in the Gliese-876 planetary system, *Mon. Not. R. Astron. Soc.* **460**, 1094 (2016).
- [10] R. Alves Silva, C. Beaugé, S. Ferraz-Mello, P. M. Cincotta, and C. M. Giordano, Instability times in the HD 181433 exoplanetary system, *Astron. Astrophys.* **652**, A112 (2021).
- [11] P. M. Cincotta, C. M. Giordano, R. Alves Silva, and C. Beaugé, The Shannon entropy: An efficient indicator of dynamical stability, *Physica D* **417**, 132816 (2021).
- [12] P. M. Cincotta, C. M. Giordano, R. Alves Silva, and C. Beaugé, Shannon entropy diffusion estimates: sensitivity on the parameters of the method, *Celest. Mech. Dyn. Astron.* **133**, 7 (2021).
- [13] K. Tsiganis, H. Varvoglis, and R. Dvorak, Chaotic diffusion and effective stability of Jupiter Trojans, *Celest. Mech. Dyn. Astron.* **92**, 71 (2005).
- [14] B. V. Chirikov, A universal instability of many-dimensional oscillator systems, *Phys. Rep.* **52**, 263 (1979).
- [15] I. I. Shevchenko, *Dynamical Chaos in Planetary Systems* (Springer, Cham, Switzerland, 2020).
- [16] P. M. Cincotta, C. M. Giordano, and I. I. Shevchenko, Revisiting the relation between the Lyapunov time and the instability time, *Physica D* **430**, 133101 (2022).
- [17] V. I. Arnold, On the nonstability of dynamical systems with many degrees of freedom, *Dokl. Akad. Nauk SSSR* **156**, 9 (1964).
- [18] P. M. Cincotta, C. M. Giordano, J. G. Martí, and C. Beaugé, On the chaotic diffusion in multidimensional Hamiltonian systems, *Celest. Mech. Dyn. Astron.* **130**, 7 (2018).
- [19] A. Giorgilli, in *Les Methodes Modernes de la Mecanique Celeste*, edited by D. Benest and C. Froeschlé (Frontières, 1990), p. 249.
- [20] N. N. Nekhoroshev, An exponential estimate of the time of stability of nearly-integrable Hamiltonian systems, *Russ. Math. Surv.* **32**, 1 (1977).
- [21] P. M. Cincotta and C. M. Giordano, Phase correlations in chaotic dynamics: a Shannon entropy measure, *Celest. Mech. Dyn. Astron.* **130**, 74 (2018).
- [22] C. M. Giordano and P. M. Cincotta, The Shannon entropy as a measure of diffusion in multidimensional dynamical systems, *Celest. Mech. Dyn. Astron.* **130**, 35 (2018).
- [23] B. V. Chirikov, Patterns in chaos, *Chaos, Solitons Fractals* **1**, 79 (1991).
- [24] I. I. Shevchenko, Marginal resonances and intermittent behavior in the motion in the vicinity of a separatrix, *Phys. Scr.* **57**, 185 (1998).
- [25] I. I. Shevchenko, On the maximum Lyapunov exponent of the motion in a chaotic layer, *JETP Lett.* **79**, 523 (2004).
- [26] P. M. Cincotta and C. M. Giordano, Theory and applications of the mean exponential growth factor of nearby orbits (MEGNO) method, *Lect. Notes Phys.* **915**, 93 (2016).
- [27] P. M. Cincotta and C. Simó, Simple tools to study global dynamics in non-axisymmetric galactic potentials-I, *Astron. Astrophys. Suppl. Ser.* **147**, 205 (2000).
- [28] P. M. Cincotta, C. M. Giordano, and C. Simó, Phase space structure of multi-dimensional systems by means of the mean exponential growth factor of nearby orbits, *Physica D* **182**, 151 (2003).
- [29] G. Benettin, L. Galgani, A. Giorgilli, and J. M. Strelcyn, Lyapunov characteristic exponents for smooth dynamical systems; a method for computing all of them, *Meccanica* **15**, 9 (1980).
- [30] C. Simó, Global dynamics and fast indicators, in *Global Analysis of Dynamical Systems*, edited by H. W. Broer, B. Krauskopf, and G. Vegter (IOP, Bristol, UK, 2001), p. 373.
- [31] E. Hairer, S. Norsett, and G. Wanner, *Solving Ordinary Differential Equations I: Nonstiff Problems* (Springer-Verlag, 1987).
- [32] P. Prince and J. Dormand, High order embedded Runge-Kutta formulae, *J. Comput. Appl. Math.* **7**, 67 (1981).
- [33] C. Simó and C. Valls, A formal approximation of the splitting of separatrices in the classical Arnold's example of diffusion with two equal parameters, *Nonlinearity* **14**, 1707 (2001).